Preliminary investigations for the development of a detector system

Externally measuring the amount of activity in the blood

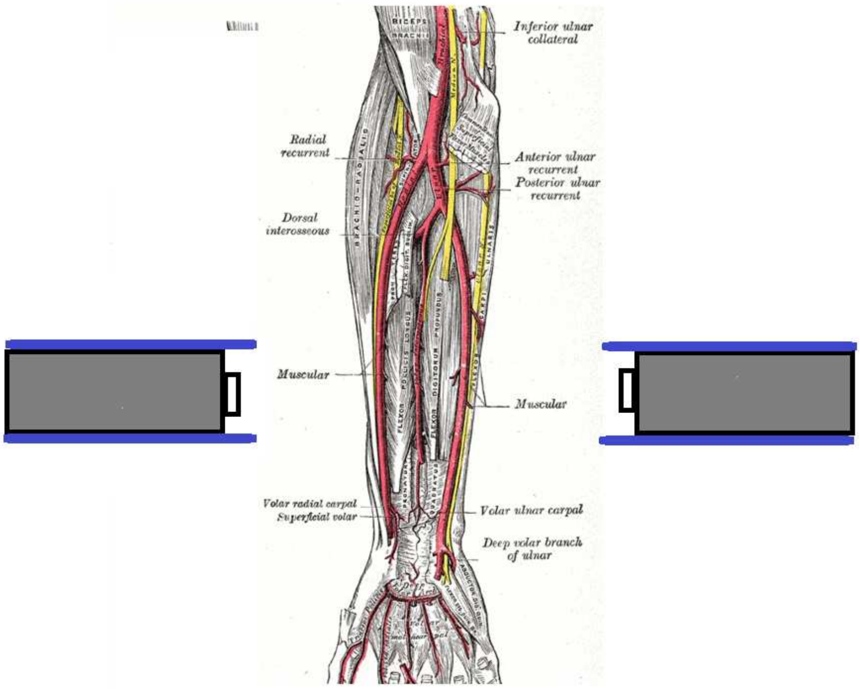

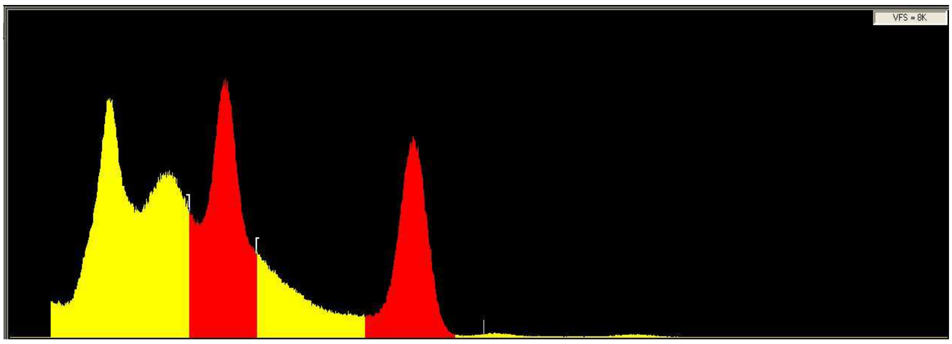

Rory M.S. de Zanger

08027803

thesis

Applied physics (B Eng)

Proem

The thesis that lies before you is the result of undergraduate research conducted at both the Delft University of Technology (TUD) and the Erasmus University Medical Center Rotterdam(EUMCR). At the TUD research was conducted at the department of Radiation, Isotopes and Health (RIH) which is located in the Reactor Institute Delft (RID) and is a part of the faculty of applied sciences. At EUMCR research was conducted at the Department of Nuclear Medicine.

First of all, I would like to thank the colleagues at the RIH for their warm welcome. In particular I would like to thank Dr. Ir. Peter Bode for the opportunity to fulfill my undergraduate research at the RIH. In addition, I would like to thank him for his guidance during my research and sharing his knowledge and intellect with me.

I would also like to thank Boxue Liu, MSc for his guidance during my research and for sharing his knowledge and intellect with me. I also would like to thank him for the discussions we had that led to better understanding of the project.

My appreciation and thanks also go out to Dr. Dan DeVries for reviewing my thesis concerning English and of course sharing his knowledge on specific physical principles.

From the EUMCR I would like to thank Dr. Wout Breeman for the opportunity to do experiments at the department of Nuclear Medicine and his assistance with some experiments.

Finally, I would like to thank Ing. Jan van Yperen and Ir. Gerard van Woggelum for being my undergraduate supervisors at the Hague University of Applied Sciences. I would also like to thank them along with Dr. Ir. A. Volker for being in the undergraduate committee overseeing my thesis defense.

Abbreviations

EUMCR	Erasmus University Medical Center Rotterdam
eV	electron volt
FOV	Field of View
GEP NET	Gastro entero pancreatic neuro endocrine tumor
MCA	Multi Channel Analyzer
MCNP	Monte Carlo N Particle transport code
mL	milliliter
p.i.	Post Injection
PMT	Photomultiplier tube
PPRT	Peptide Receptor Radionuclide Therapy
RID	Reactor Institute Delft
RIH	Radiation, Isotopes and Health
SNR	Signal-to-Noise Ratio
TUD	Delft University of Technology

Abstract

PRRT is a method of treatment that is used for a variety of diseases. In this method of treatment patient are infused with a radiopharmaceutical. This radiopharmaceutical will deliver a radiation dose to the specific targeted organ. However, due to infusion in the bloodstream other organs will also sustain a radiation dose like for example the bone marrow. There is a method to determine the radiation dose sustained by the bone marrow. This method requires that the amount of activity in blood is determined for several moments in time. Currently this is done by taking blood samples from patients and measuring these samples in dose calibrators.

Theoretically, it should be possible to measure the amount of activity in blood by means of external measurements. These measurements could be performed by using two oppositely positioned $CeBr_3$ scintillation detectors that are linked to photomultiplier tubes. However, before these measurements could be conducted preliminary investigations were necessary. These preliminary investigations were described in this thesis.

Preliminary investigations were conducted on several criteria. These criteria ranged from position of the detector system to detector properties. In specific, the optimal detector system position with respect to the body, and with respect to the arm was determined. The detector properties that have been investigated were detector linearity, detector response and detector linearity. In addition, investigations on SNR and shielding have been conducted.

Experiments and simulation showed that the optimal position for the detector system is at wrist position with the arm extended sideways as far as possible. It has also been shown that the optimal position for the detectors with respect to the arm is at a distance of 10 cm between detectors and arm. With this detector position the signal-to-noise ratio can be improved by use of shielding. With 1.60 cm thickness of lead shielding the SNR will not become lower than 100. In addition, it has been shown that the detector properties for both detector is nearly similar.

These investigations led to promising results. The results show a specific set-up for the detector system with which the amount of activity in blood could be determined by means of external measurements.

Content

1. Introduction

Radionuclide therapy is a (well) known method for treatment of a variety of deceases. The key aspect of the treatment is targeted radiation of tumors, metastases or organs. An example of radionuclide therapy is peptide receptor radionuclide therapy (PRRT). In the Erasmus University Medical Center Rotterdam (EUMCR), at the department of Nuclear Medicine, PRRT is used for the treatment of gastro entero pancreatic neuro-endocrine tumors (GEP NETs) among others [1,2].

The radiopharmaceutical for this specific treatment is a radio-labeled peptide called [^{177}Lu-DOTA^{0},Tyr^{3}]-Octreotate, which is administered via infusion. The radiopharmaceutical will accumulate in tumor(s) and metastases and deliver a radiation dose to these tissues. Moreover, internal organs will also sustain a certain radiation dose e.g. bone-marrow.

Bone-marrow is the most radiosensitive organ in the body and is therefore a dose limiting organ in radionuclide therapy. For health and treatment purposes it is vital to know the dose sustained by the bone-marrow during and after treatment. The radiation dose to the bone marrow is directly related to the amount of activity in the blood [3]. In order for bone marrow dosimetry to become possible quantitative radiation measurements of blood are necessary.

Generally, the amount of activity in the blood is determined by taking blood samples at different set times after infusion and measuring these samples. However, this method is very imposing on the patient and also introduces additional radiation risk for the staff. The tolerated radiation dose for staff is 5 mSv/year. In order to avoid these circumstances a method has to be developed in which the amount of activity in the blood can be determined without taking blood samples. This system should then reduce the radiation dose to 1% of the annual year dose. Thus, the yearly radiation dose should become 0.05 mSv/year.

As a consequence, all measurements need to be performed from outside of the body. These measurements require a detector system that is able to measures radiation qualitatively and quantitatively. This detector system could then be placed at a well perfused extremity e.g. underarm/wrist and measure the amount of activity in the blood.

Since there is no detector system commercially available for this specific purpose the detector system has to be developed [Appendix A].

2. Project Overview

2.1. Introduction

PRRT is a method of therapy for a variety of deceases. In PRRT patients are treated by infusion of radionuclide linked antibodies or peptides. Although this method of treatment proved to be successful for many patients, it is accompanied by certain disadvantages. One of these disadvantages, probably the most important disadvantage, is the dose delivered to healthy organs. The dose that healthy organs may receive is limited. Above this dose limit radio toxicity will occur. Dose required to cause radio toxic effects differs for each organ. Organs that show radio toxic effects at a low dose are called radiosensitive organs. These radiosensitive organs will determine the maximum administrable dose.

Radio toxic effects can be prevented by not exceeding the dose limit of the most radiosensitive organ. However, in treatment it is desired to maximize dose. Thus, optimization of treatment requires accurate determination of delivered dose called dosimetry.

Adequate dosimetry requires the determination of amounts of activity in the body, that is the amount of activity in organs, blood and the remainder (other soft tissues). In this project focus will lie on determining whether the amount of activity in blood can be determined using external measurements.

External measurements on the amount of activity in the blood could then replace the current method in which blood samples are taken from patients and measured. This latter method is rather invasive on patients and increases radiation risk for medical personnel.

2.2. Problem description

The amount of activity in blood has to be determined by means of external measurements to lower radiation dose to staff. These measurements will be subject to several criteria:

1. Patient comfort
    a. Detector system positioning with respect to the body of the patient
    b. Detector positioning with respect to the forearm/wrist
2. Interference from other radiation sources (Noise)
    a. Leakage of incident photons from outside the field of view
    b. Background radiation
3. Reproducibility[1]
4. Weight of the detector system

One of the purposes of this detector system is to make measurements less invasive and inconvenient for patients. Comfort for patients during external measurements will depend optimal positioning of the detector system with respect to the patient. In addition, this optimized positioning would also serve another purpose.

Measurements to determine the amount of activity in the blood should be conducted without measuring activity from any other source. Radiopharmaceuticals will be distributed in the body after infusion. Thus, organs, bone and other soft tissues (remainder) will also contain a certain amount of activity. Incident photons emitted by the activity in these tissues might be detected by the detector system and thereby interfere with measurements (noise). Minimization of this interference also requires optimized placement of the detector system with respect to the patient's body.

[1] These criteria are not

With the detector position optimized and background interference minimized there still is another source of interference. This interference is not to be classified as noise however, it does make accurate quantitative measurements difficult. It will cause more activity to be detected in the field of view and therefore overestimate the activity. In addition, correct assessment of the volume of blood that has been in the field of view will not be performed correctly. These two inaccuracies will increase the error in determining the volume activity of the blood.

Measurements on the amount of activity might be conducted accurately however, this does not automatically mean that the measurements can also be conducted reproducible. The reproducibility of measurements depend on criteria like changing positions during or subsequent measurements. Change in any criteria should be minimized or compensated for during measurements.

2.3. Project design requirements

The development of the detector system can be regarded as successful once the amount of activity in the blood can be determined with a accuracy of ± 10% from the . For this to become feasible the detector system should meet certain requirements. These requirements for the detector system are based on the previously described problem description.

The detector system will be used for measurement of ^{177}Lu but might also be used to do measurements on other gamma emitting radionuclides. Due to this, the detector system should be able to measure a gamma spectrum. This requires the usage of one or more gamma ray detectors that can simultaneously quantify the energy of the incident photons and a multichannel analyzer. This leaves a variety of detectors possible. The type of detector used during this project is a scintillation detector with a photomultiplier tube.[2]

Determining the amount of activity in the blood requires the detectors to be focused on blood vessels (arteries and veins) without having to much other tissues (bone, organs and other soft tissues) in the vicinity that might contain activity or attenuate the photons emitted from the blood. In addition, incident photons emitted from the rest of the body should not be detected with the detector system. These requirements can be met by placing the detectors at forearm/wrist position. In addition, the detectors should be collimated and shielded from other radiation sources.

Measurement should be conducted with a certain accuracy and reproducibility. Reproducibility requires the use of two detectors within the detector system. It also requires a specific set-up for these detectors. The detectors should be placed opposite from each other with a set space between them. This set-up of the detector will make it possible reduce or correct for the variation of positioning of the source. Moreover, the set-up will make it also possible to correct for anisotropic properties of the source.[4]

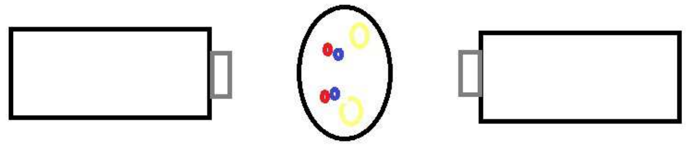

Figure 1. Schematic representation (cross section) of the set-up for wrist measurement.

[2] This type of detector was already available to use in this project.

Shielding and collimating the detectors may meet requirements however, optimal positioning of the detector system will also reduce noise. The position of the detector system does not have to be changed with respect to the body (detector system may be kept at wrist position). It can also be changed with respect to the entire patient. The detector system is required to have a minimal weight. This requirement can be met by this optimizing of the positioning of the detector system with respect to the patient. It will reduce noise, as stated earlier. Thus reducing the amount of shielding needed. The detector system can then be made relatively lighter.

2.4. Objectives

The objectives of this project can be summarized into a number of questions. It will probably not be possible to answer all questions. This is due to the limited amount of time available to conduct this project. Important question for this project are:

1. What will be the optimal position for the detector system with respect to the body?
    a. Why is this the optimal position?
2. Will this optimal position of the detector system create a desirable SNR?
3. Is it possible to increase the SNR?
4. How can this SNR be improved?

These first few question are of a more theoretical nature. There will also be question that can only be answered after

5. Do the detectors show a linear response for a range of activities?
6. With what efficiency will the detectors measure the 113 keV and 208 keV photons?
7. Is it possible to alter the FOV of the detectors with a simple geometry of shielding?
8. How can leakage of photons outside of the field of view be prevented?

These question will be answered by means of simulations and experiments. In specific, the positioning of the detector system will be determined after simulations conducted with Microshield®. Simulations will also be conducted to determine the fluence rate at detector position for a geometry that will represent the wrist/forearm. All these simulation results will be used in investigation on the SNR.

Measurements will be conducted to determine the linearity, response and efficiency of the detectors. In addition, the shielding will be applied to the detectors to determine whether the FOV can easily be altered and determine the effects of leakage for the specific geometry of shielding.

3. Theory

In the development of a detector system a sound knowledge of related physical principles is needed. A proper understanding of these principles will create the opportunity to make educated choices to the design for the detector system. In addition, experiments can be designed correctly and conducted accurately. The theoretical foundation of these physical principles are described in this chapter. The subjects that are described are:

1. Gamma ray interactions with matter
    - Photoelectric effect
    - Compton effect
    - Pair production
2. Attenuation of gamma rays
3. Self attenuation
4. Detection and measurement of ionizing radiation
5. Propagation of errors.

3.1. Gamma ray interactions with matter

Gamma rays (photons) will interact with matter. However, the probability for interaction of photons with matter are relatively low. Once interactions between photons and matter occur the transferred energy is generally considerable. Photons may interact with various objects within an atom. The objects with which interactions may occur are an atomic nucleus, atomic bound electrons or electrical fields caused by the nuclei and electrons. The amount of energy transferred during interactions varies from no energy transferred to all photon energy transference resulting in their disappearance.

The mechanisms for interactions between photons and matter can be reduced to three primary ones: photoelectric effect, Compton scattering and pair production. There are other interaction mechanisms that may occur. However, these do not occur as frequently and prove to have a negligible effect.

The occurrence of interaction mechanisms depend on the energy of the incident photon. Moreover, the occurrence of interaction mechanisms also depends on the atomic number of the material with which it occurs. These characteristics have been depicted in figure 1. In figure 1 can be seen which interaction mechanism will occur most frequently for photon energies and atomic numbers of materials.

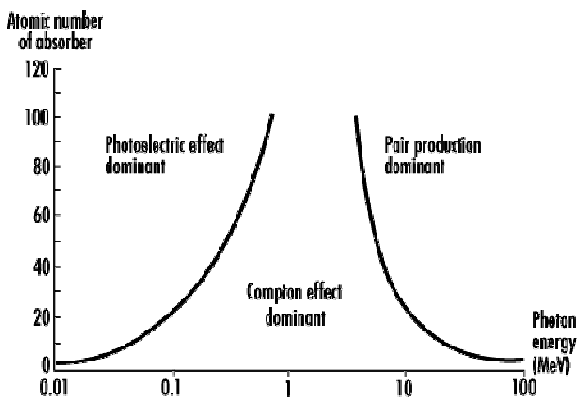

Figure 2. The figure shows a graph in which the atomic number is plotted as function of the photon energy. In the graph the relation between mechanisms for interaction and photon energy can be seen.

3.1.1 Photoelectric effect

An incident photon with energy E_γ may interact with an atomic electron. The interaction can be described as a collision between photon and electron that will result in a transfer of E_γ to the electron. Due to this energy transfer during the collision the photon ceases to exist and the electron is emitted from the atom. That is, if the energy of the photon is greater than the binding energy E_b of the electron. The emitted electron will have a certain kinetic energy $E_{k,e}$. Kinetic energy of the emitted electron can be calculated by subtracting the binding energy of the electron from the photon energy:

$$E_{k,e} = E_\gamma - E_b \tag{1}$$

Momentum is conserved during the entire process.[4]

3.1.2 Compton effect

The Compton effect can also be described as a collision between a photon and an electron. An incident photon with energy E_γ interacts with an electron in which E_γ is not fully transferred. The energy of the incident photon is divided between the electron and photon, reducing the incident photon in energy and increasing the kinetic energy of the electron. Photons which energy have been reduced due to collisions with matter are called scattered photons.

The distribution of energy between a scattered photon and the Compton electron is directly related to the angle between incident photon and the scattered photon. An equation can be derived for both the E_γ and E_e. From these equations it becomes clear that the Compton-electron will never absorb all of the energy of the incident photon. In addition, both equations comply with the law of energy conservation can easily be observed since:

$$E_\gamma = E_\gamma^{'} + E_e \tag{2}$$

Another relationship between angle of scattering and energy of incident photons can be found. This relationship can be made clear by making an polar diagram. This diagram can be seen in figure 3:

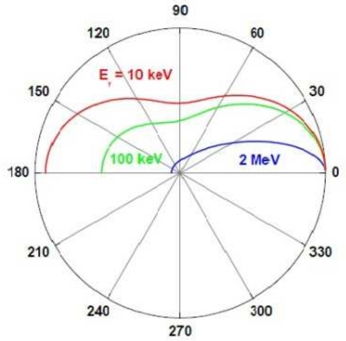

Figure 3. Polar diagram of the angle of scattering of the scattered photon for different photon energies.

In the polar diagram of figure 3 the energy of the incident photon is plotted as a function of the angle of scattering. In the diagram, the angle is shown along the edge of the circle. From the polar diagram can be read what the angle of scattering is for different photon energies. In can be seen that the angle of scattering decreases as the energy of the incident photon increases.

3.1.3 Pair production

Pair production is an interaction mechanism of photons and the nuclei of atoms. In this mechanism incident photons will be converted to a particle-antiparticle pair e.g. an electron-positron pair. However, this conversion may only occur when the incident photon has sufficient energy to create these particles. For the creation of an electron-positron pair the required energy of the photon has to be greater than two times the mass of an electron (1.022 MeV/c^2):

$$h\upsilon > 2m_e c^2 \tag{3}$$

Where h is the constant of Planck: 6,63· 10^{-34} [J·s], v is the frequency of the incident photon [Hz], m_e is the mass of an electron:9.11 · 10^{-31} [kg] and c is the speed of light [m·s^{-1}].

Any remaining energy will be transferred to each particle as kinetic energy. Both particles will move away from the production site in a strong forward motion. During their travel they will lose energy due to collisions. Eventually the positron will annihilate with an electron. With this annihilation two photons will be produced, each having an energy of 511 keV. These photons will be emitted from the annihilation site in opposite direction [6].

NB. As stated, pair production requires high photon energies (>1022 keV). ^{177}Lu does not emit any high energy photons. Thus, pair production is not an issue in this thesis.

3.2. Attenuation of gamma rays

It should be clear that attenuation of gamma rays is caused by interactions with matter. In addition, it should be clear that interactions between gamma rays and matter is subject to chance. By increasing the thickness of a material the chance for gamma rays to interact will also increase, and so the exiting intensity will decrease even more. In other words, the change in intensity ΔI is proportional to thickness x and the incident intensity I_0:

$$\Delta I = \mu I_0 \Delta x \tag{4}$$

Where μ is the proportionality constant and is known as the attenuation coefficient [7]. For a homogeneous distributed radiation source the absorption coefficient is constant. In this case integration of equation 4 becomes easy and the equation yields:

$$I_x = I_0 e^{-\mu x} \tag{5}$$

Equation 5 gives the remaining intensity I_x of an initial radiation beam I_0 that has traversed through thickness x of a particular material. It should be stated that due to the negative exponential character of the attenuation the remaining gamma ray intensity will never become zero.

It should also be stated that the degree of attenuation depends on the material used to attenuate gamma rays. Material dependency is incorporated into the attenuation coefficient since the attenuation coefficient is defined as:

$$\mu \stackrel{\text{def}}{=} N\sigma \tag{6}$$

where N is the number of atoms and σ is the cross section expressed in barns. The cross section defines the probability for interaction to occur. For multiple materials this will become:

$$\mu = \sum N_i \, \sigma_i \tag{7}$$

The attenuation coefficient μ shown in equation 6 is defined as the linear attenuation coefficient and is expressed in cm^{-1}. The number of atoms can be calculated by:

$$N = \frac{\rho N_A}{M} \tag{8}$$

where ρ is the density of the material in $g \cdot cm^{-3}$, N_A is the Avogadro's constant in mol^{-1} and M is the molar mass of the element or compound in $g \cdot mol^{-1}$. Equation 8 shows the dependency of material due to the density term in this equation.

The attenuation coefficient has been defined as the linear attenuation coefficient. However, it is also possible to define the attenuation coefficient differently i.e. as a mass attenuation coefficient. Mathematically this mass attenuation coefficient is given by:

$$\frac{\mu}{\rho} = \frac{N_A \sigma}{M} \tag{9}$$

where μ/ρ is the mass attenuation coefficient, usually expressed in $cm^2 \cdot g^{-1}$. This mass attenuation coefficient can be used to compare the attenuating properties of different materials and thus for different density. This can be done since the density is used in the equation as can be seen in equation 9 and later equation 10.

To calculate the intensity of a radiation beam that has traversed through a material using the mass attenuation coefficient equation 5 has to be modified slightly:

$$I_x = I_0 e^{-(\frac{\mu}{\rho})\rho x} \tag{10}$$

It should be stated that equations 5 and 10 are only valid for narrow beam radiation. In a narrow beam the photons will pass through the material without interacting with the material or interact with the material without causing scattered photons. In addition, scattered photons will not reach the detector. Thus, the distance traveled by photons in a narrow beam is nearly equal for all photons. In presence of a narrow beam the difference in intensity between before and after passing through material is a proper representation of the stopping power or attenuating properties of a material.

Build up

It should be stated that in practice a narrow beam of photons occurs very seldom. Usually the geometry of the photon beam is more wide, also called broad beam geometry. The broad beam of photons is attenuated as described above. However, in this broad beam of photons there is a contribution of scattered photons. This is called build-up. The contribution of scattered photons can be calculated and is called build-up factor *B*. The build-up factor is determined by the geometry of the source and the attenuating material.

3.3. Self attenuation

Photons are easily emitted from a radiation source with no measurable dimensions i.e. a point source. The same applies to radiation sources with small dimensions. However, with increasing dimensions of the radiation source the probability of interactions between emitted photons and other atoms within source increases. Photons that in fact interact within the radiation source will be attenuated with the same interaction mechanisms as described in paragraph 3.1. This type of attenuation is called self attenuation.

Self attenuation results in deviations between true amount of activity and measured amount of activity, where the true amount of activity will be underestimated. These deviations increase as the volume of the source increases. The reason for this can be found in the distance each photons has to travel through the source. Photons on the edges of the source will leave the source without or with minimal interactions and are therefore easily measurable. However, photons emitted from the center of the source or from the edge of the source in direction of the other edge have to travel a large distance through the source and will be attenuated. An example of this principle is depicted in figure 4.

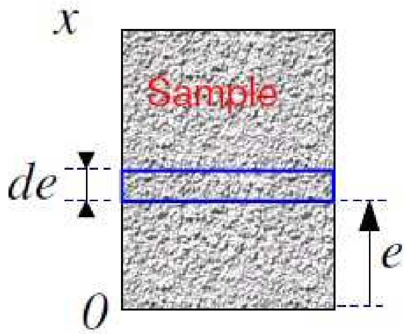

Figure 4. Example of a sample source in which is shown that the photon attenuation has to be calculated over the distance travelled by the photon.

The self attenuation within a source is calculable. An equation can be derived for the measurable intensity by integrating equation 5 over the distance travelled by the photons [8]. The resulting equation is presented here:

$$I_x = I_0 \frac{1-e^{(-\mu x)}}{\mu x} \tag{11}$$

Equations 5, 10 and 11 can also be expressed for photon fluence (Φ) or fluence rate (ϕ).

3.4. Detection and measurement of ionizing radiation

3.4.1 The detection of ionizing radiation

The detection of ionizing radiation is based on proving the presence of said radiation. During the detection of ionizing radiation quantitative information on certain parameters is often also gathered. These parameters may include fluence rate, dose and energy.

The detection of ionizing radiation, both qualitative and quantitative, is based on the process of interactions between radiation and detector material. During these interactions the radiation energy will mostly be absorbed. The interactions will subsequently result in a conversion into processable signals like electricity or light. There are systems in which the signal output is an average effect over time for relatively many interactions. However, in most cases the effect of each individual radiant quant is processed and recorded. This method of measurement can be characterized as counting, in which the stochastic properties of radioactive decay are expressed.

Stochastic properties of radioactive decay are a result of the randomness during decay. In term, measurements on radioactive sources are also stochastic in nature. This stochastic nature of detection can be described using statistics.

3.4.2 Statistics of radioactive decay

Radioactive decay of atoms is a random process. As a consequence, radioactive decay of a single atom and its nucleus is also a random process. This random process can be described mathematically using statistics. In this process there are two outcomes possible: there is a chance p that the nucleus will decay within a certain amount of time and there is a chance $1-p$ that this will not happen.

Radioactive decay of a single nucleus will not influence or initiate the decay of any other nuclei. In other words, the decay of a nucleus is independent from the decay of other nuclei. Thus, the decay of nuclei can be considered as repetitions of the decay of a single nucleus. The binomial probability distribution can be used to describe this principle since it describes the probability for k successes with n repeated processes that each has two possible outcomes. Mathematically this can be expressed as follows:

$$P(k) = \frac{n!}{k!(n-k)!}\, p^k (1-p)^{n-k} \tag{12}$$

This probability distribution has an expected value: $\mu = np$, and a standard deviation of: $\sigma = \sqrt{np(1-p)}$. This distribution is generally valid for experiments involving counting. In most cases the number of decays is relatively high. Consequently, n will be relatively high. This will make calculations on this specific type of probability distributions rather complicated. However, for large number of n ($n \rightarrow \infty$, $p \rightarrow 0$) the binomial probability distribution will transition into the mathematically simpler Poisson probability distribution:

$$P(k) = \frac{\lambda^k}{k!} e^{-\lambda} \tag{13}$$

Where the expected value $\mu = \lambda$, and the standard deviation is given by $\sigma = \sqrt{\lambda}$. As can be seen, the distribution for these types of experiments are characterized on one parameter, the expected value λ.

For large values of this expected value λ the distribution will narrow. In this case, the Poisson distribution can be approximated by a normal (Gaussian) distribution. Mathematically the normal (Gaussian) distribution can be expressed as follows:

$$P(k) = \frac{1}{\sqrt{2\pi\lambda}}\, e^{\frac{-(k-\lambda)^2}{2\lambda}} \tag{14}$$

Where the expected value λ and standard deviation σ is similar to expected value and standard deviation used in the Poisson probability distribution. This shows that both binomial probability distributions and Poisson probability distribution can be used to determine the standard deviation in measurements. The Poisson probability distribution is preferred since the mathematics for this distribution is easier.

3.4.3 Parameters in measuring activity

In a counting experiment where a number N is counted both Poisson and normal (Gaussian) probability distributions will result in the following expected value and standard deviation:

$$\bar{x} = N \tag{15}$$

$$s = \sqrt{N} \tag{16}$$

The results will show a 68% probability that the mean will lie between $\bar{x} \pm s$. This probability increases when the standard deviation is increased. This gives a 99,7% probability that the mean will lie between $\bar{x} \pm 3s$.

Rate

Measurements on radioactive decay can be performed by merely counting the number of detected particles and/or photons N. However, it is also possible to determine the rate R with which particles or photons are detected. This rate is defined as the number of particles and/or photons detected within a certain period of time or measuring time t:

$$R = \frac{N}{t} \tag{17}$$

This measuring method, like any other measuring method, will be accompanied by a specific uncertainty. The uncertainty in the rate ΔR is determined by the uncertainty in the number of detected particles/photons ΔN and the uncertainty in the measuring time Δt. However, the measuring time is assumed to be determined precisely with a relative inaccuracy of about $1.0 \cdot 10^{-4}$ %. Therefore, contribution to the uncertainty in the rate will be negligible. The uncertainty in the rate will then be only determined by the uncertainty in the number of the detected particles/photons:

$$\Delta R = \frac{\Delta N}{t} = \frac{\sqrt{N}}{t} = \sqrt{\frac{R}{t}} \tag{18}$$

Background radiation corrections

Any quantitative measurement on radiation sources are gross measurements. That these measurements are gross measurements is due to the origin of the measured activity. The measured amount of activity is a combination of activity originating from the radiation source and activity originating from any other source, usually referred to as background radiation.

Correct quantitative measurements on a radiation source are conducted by performing a background radiation subtraction. This is done by measuring the radiation source S and the background radiation B separately. Subsequently, the B is subtracted from S. Usually the measurement time for both the B and S is different. By using the rate R, the variable of time is compensated for. Thus, both measurements are expressed in a rate R.

$$R_{net} = R_S - R_B \tag{19}$$

Where R_{net} is the true rate of the radiation source.

3.4.4 Scintillation detector

There are chemical elements or compounds that have a luminescent property. Luminescent chemicals emit light after absorbing energy. A scintillator exhibits this luminescent property after absorbing energy from ionizing radiation. Light emitted due to the luminescence has an intensity that is proportional to the absorbed radiation energy.

The absorption of radiation energy will excite the detector material, i.e. the chemical (compound), to a heightened energy state. Eventually the chemical will be relaxed back into a lower or even ground energy state and hereby emit light in a very short pulse. The time between absorption and emission of energy may vary from picoseconds to hours. Generally, the time between these two events is rather short (microseconds).

The scintillation crystal is (usually) connected to an optical light detector. In most cases this light detector is a photomultiplier tube (PMT). The PMT receives the light pulses emitted by the scintillation crystal, multiplies the light signal and converts it into a measurable voltage signal. A schematic representation of a scintillation detector and PMT is shown in figure 5.

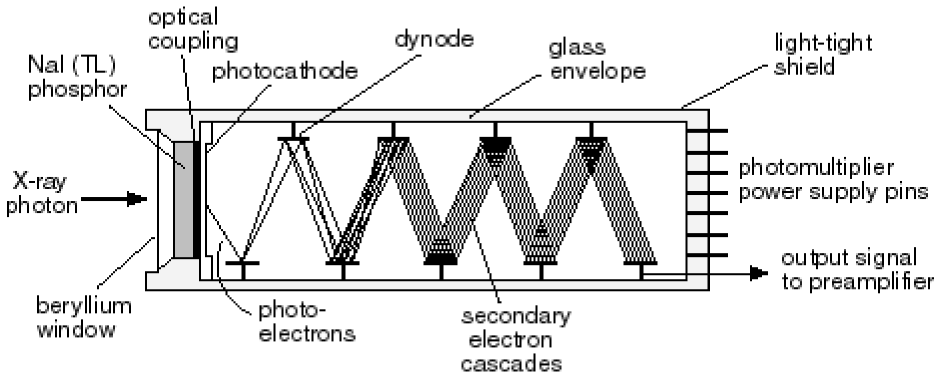

Figure 5. Schematic representation of a scintillation detector (scintillation crystal and PMT).

The scintillation crystal is of the essence when it comes to these types of the detectors. Each type of scintillation crystal has specific properties. One of these properties is the ease with which radiation energy can be absorbed also referred to as stopping power. In addition, the sensitivity and the intensity of the emitted light are also scintillation crystal i.e. chemical specific.

The stopping power of a crystal will determine the detection efficiency of various photon energies and influence the crystal size. Greater stopping power results in the fact that less thickness of crystal is needed to create adequate signal. A small thickness of crystal is preferred since a great thickness has a negative effect on energy conversion. The light pulse that has been created during absorption of energy might be extinguished before it can reach the PMT. Once this process occurs to often this can have negative effects on the signal. In other words, the signal will be underestimated.

3.5. Propagation of errors

Measurements can never be conducted perfectly. There is always an uncertainty in the measurement. The uncertainty is expressed in a value that encloses the measured value and shows the range in which the true value will lie. This uncertainty will always be expressed at a certain degree of accuracy. Here is an example of measured amount of activity in a radiation source including the uncertainty The degree of accuracy shown here is 1σ.

A = (0.5 ± 0.1) MBq

Suppose that this amount of activity is measured using a dose calibrator and that this amount of activity in used in another measurement with a different detector. Measurements with the second detector will also be conducted with an uncertainty. Thus, this second measured value is also accompanied by an uncertainty. The uncertainty in the final value is based on uncertainties in both measurements. This is called propagation of errors.

In general, for each performed measurement the error is propagated. Thus, the uncertainty in the final measured value is based on the uncertainty in all correlated measurements. A general mathematical model has been created that can be used to calculate the uncertainty in a variable that is based on other variables, each with their own uncertainty.

Suppose that a f is a function of three variables: x, y and z. The uncertainty in f can then be given by:

$$\Delta f(x,y,z) = \left|\frac{\partial f}{\partial x}\right| \Delta x + \left|\frac{\partial f}{\partial y}\right| \Delta y + \left|\frac{\partial f}{\partial z}\right| \Delta z \quad (20)$$

The method used in equation 20 can be applied for any number of variables in any type of measurement. There is an easier method of calculating the uncertainty and is shown here:

$$s_C = \sqrt{{s_A}^2 + {s_B}^2} \quad (21)$$

Where s_A is the uncertainty in measurement A, s_B is the uncertainty in measurement B and s_C will then be combined uncertainty of the two measurements. This method is a relatively accurate approximation and is a proper alternative for equation 20.

4. Optimal positioning of the detector system

4.1. Introduction & objective

In the developing stage of the detector system the optimal positioning for the detector system has to be investigated. The optimal position for the detector system will depend on comfort for the patient and minimizing interference from background radiation. Thus, the aim is to determine this position.

4.2. Theoretical foundation

Optimizations on the positioning of the detector system is based on the premise that the photon fluence varies for different positions around a radiation source. This premise is based on the fact that the photon fluence is defined as:

$$\Phi = \frac{dN}{dA} \qquad (22)$$

Where Φ is the photon fluence [m^{-2}], N the number of photons [-] and A is the surface area [m^2]. Equation 23 can be used to show that the photon fluence decreases as the distance to the source increases since:

$$\Phi = \frac{N}{4\pi r^2} \qquad (23)$$

Where r [m] is the distance to the source. It should be mentioned that this applies to sources that are isotropic in nature like point sources[3] and spherical sources that have negligible dimensions. However, the body is a complex geometry that is certainly not isotropic in nature. Even if the activity is distributed in the body homogeneously, the geometry will not be isotropic in nature. This suggests that the premise is indeed true.

In this chapter the fluence rate will be used instead of the photon fluence. This fluence rate is defined as followed:

$$\phi = \frac{d\Phi}{dt} \qquad (24)$$

Where ϕ is the fluence rate [$m^{-2} \cdot s^{-1}$] and t is time [s].

4.3. Methods and materials

Microshield® has been used to conduct all simulation in this thesis. Microshield® is a simulation program that allows users to calculate several parameters involving radiation. These parameters are activity, fluence rate, energy fluence and dose rate. All parameters can be calculated for specific geometries and radionuclides and thus photon energies. In addition, Microshield® provides the opportunity to calculate all the before mentioned properties in presence of shielding.

Determining the fluence rate as a function of position around the body

Investigations were started by determining whether the fluence rate of photons originating from the body is position specific. This investigation was conducted by varying the height, width or distance with respect to the body. For these parameters (height etc) values were arbitrarily chosen since the results will be approximated by equations. These equations can then be used to calculate the fluence rate for any possible height, width or distance.

[3] A point source has no measurable dimensions.

During simulations only one variable was changed at a time. The results of these simulations would prove or disprove the hypothesis that the fluence rate varies for different position around the body. Thus, making it possible to optimize the position of the detector system in which the relatively lowest fluence rate of photons originating from the body would be measurable.

In figure 26 a schematic representation of the body has been shown in which the arm were position alongside the body. This schematic representation has been used to approximate the geometry necessary for simulations. It can be seen that the body can be approximated by a rectangular volume. Thus, this geometry was used in simulations. The dimensions used for this geometry were:

- Height: 1.8 m
- Length: 0.30 m[4] (thickness)
- Width: 1.0 m

These dimensions were arbitrarily chosen. The results will show a relative difference in the fluence rate and will therefore be the same for practically any geometry.

During simulations this rectangular volume was filled with ^{177}Lu which was distributed over geometry homogeneously (as is the case immediately after infusion of the radiopharmaceutical). Dimensions used for this geometry were:

Determining the optimal position for the detector system with respect to the body

The before mentioned simulations were followed by simulations to determine the fluence rate at specific positions. In this simulation the body was also approximated by an rectangular volume. In this case, like earlier, the geometry was based on a body in which the arm was positioned alongside the body.

In simulations, the fluence rate of photons originating from the body was determined for specific positions that would correspond to the detector system position. It was assumed that the detector system would be positioned at the wrist/forearm. In addition, it was assumed that the arm would be extended to enlarge the distance between wrist and detector system. Thus enlarging the distance between body and detector system.

The positions used in the simulations are correlated to specific arm positions. Arm positions that would be easy to maintain and comfortable for the patient. The used arm positions were:

- an extended arm forward
- an extended arm to the side.

With each arm position two parameters were varied. Parameters that have been varied were the height and the distance. During simulations the dimensions of the geometry were

NB. Figures showing the geometries used for the different arm position can be found in Appendix B1: Simulated geometries.

[4] Average patient thickness is about 30 cm. The patients are relatively thin due to the illness.

4.4. Results

Result corresponding to determination of the position dependent fluence rate

Results of the simulations on the height, width and distance dependent fluence rate are shown. In these results the fluence rate is shown for the two photon energies including build-up(§3.2):

- 113 keV
- 208 keV

The position dependent fluence rates for 113 keV and 208 keV photons both without and with build-up are shown in figures 6 to 8. Specific values used in these figures can be found in tables 1 to 3 in appendix B2.

In figure 6 the results of simulations on the fluence rate at several height positions can be seen. It can be observed that there is a slight curvature in the all lines. A proper fit for each line is obtained by applying a second order polynomial. The polynomial shows that the fluence rate varies as a function of height with respect to the geometry. These specific equations can be used to calculate the fluence rate at a random height with respect to the body.

In addition, the polynomials show that maximum photon fluencies can be observed when a detector is positioned at half height of the geometry. This applies to both photon energies, either with or without build-up. This can be explained by the fact that the path length of photons will become more equal for all photons originating from the source.

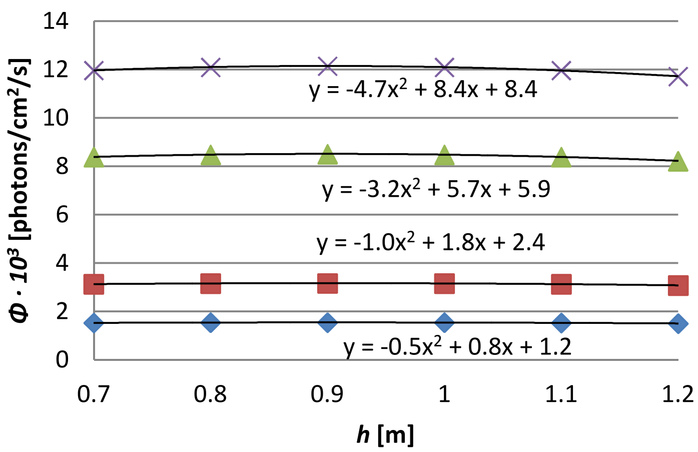

Figure 6. Graph that shows the fluence rate as a function of height. In this graph the blue line represents photons with an energy of 113 keV without build-up. The red line represents photons with an energy of 208 keV, also without build-up. The green and purple lines represents photons with energies of 113 keV and 208 keV respectively. In the latter two build-up is included.

Figure 7 shows the results of simulations on the fluence rate at several width positions. Like in figure 6, the lines show a curved shape that is best fitted with a second order polynomial. The polynomial shows that the fluence rate is also dependent on the width position with respect to the geometry. As observed from figure 6, the maximum fluence rates can be measured when detectors are positioned at half width of the geometry. All of the before mentioned observations apply to both photon energies, either without build-up or with build-up.

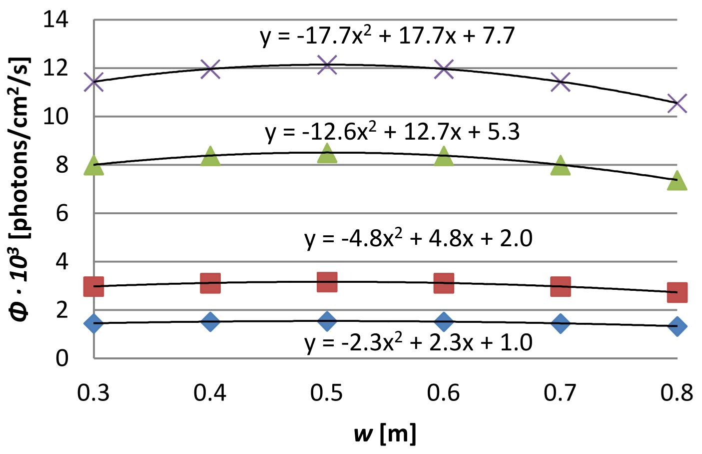

Figure 7. Graph that shows the fluence rate as a function of width. In this graph the blue line represents photons with an energy of 113 keV without build-up. The red line represents photons with an energy of 208 keV, also without build-up. The green and purple lines represents photons with energies of 113 keV and 208 keV respectively. In the latter two build-up is included.

The results of simulations on the fluence rate for several distances can be viewed in figure 8. In figure 8 it can be observed that fluence rate does not decrease with the square of the distance. This was to be expected for two reason. For one, the geometry of the source is not spherical in shape. Thus, the geometry is not isotropic in nature. Secondly, the geometry has rather large dimensions with respect to the distances used in the simulation. The source will only approximate the square of the distance for large distances between detector and source (r>>d).

It can also be seen that the decrease in fluence rate is different for both photon energies. This was to be expected since the attenuation of photons is energy specific. With increasing photon energies the attenuation will decrease. On top of that, build up also influences the decrease in fluence rate as a function of distance. This is due to the higher number of photons that will be detected for broad beam geometry as opposed to narrow beam geometries.

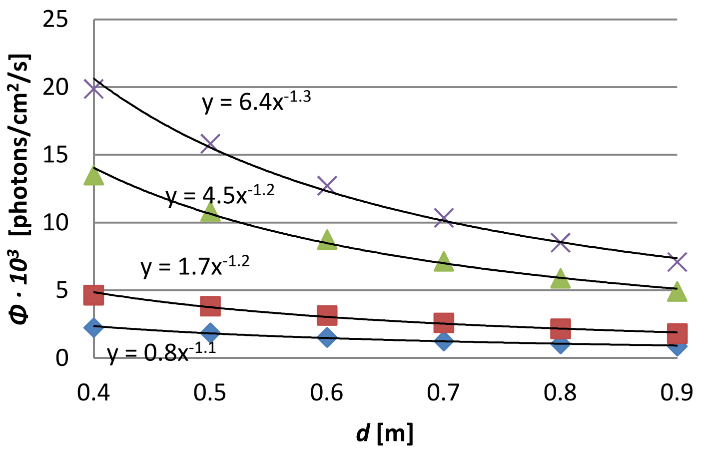

Figure 8. Graph that shows the fluence rate as a function of distance to the body. In this graph the blue line represents photons with an energy of 113 keV without build-up. The red line represents photons with an energy of 208 keV, also without build-up. The green and purple lines represents photons with energies of 113 keV and 208 keV respectively. In the latter two build-up is included.

Results presented in figures 6 to 8 show that a decrease in detectable fluence rate can be achieved by increasing the distance between geometry and detector, and positioning the detector off centre in both height and width perspective with respect to the body.

These results show that there are positions that will result in a lower measurable fluence rate. It should be possible to optimize a position for the detector system in which the measurable fluence rate of photons originating from the body will be relatively lowest.

Results associated with specific arm positions

The fluence rate of photons originating from the body was determined for the specific detector system positions. These positions are correlated to two arm positions: arm extended forward and arm extended sideways. The arm positions can be viewed in figures 27 and 28 of appendix B1. Results were obtained by conducting simulations. In addition, the height and the distance with respect to the geometry was varied.

In figure 9 the fluence rate as a function of height can be observed for the two specific arm positions. This figure shows that the fluence rate for both the 113 keV and 208 keV photon energies are significantly greater in the arm forward position. The ratio between the photon energies for both arm positions can be found in table 5 located in appendix B3.

The figure also shows that the fluence rate is at a maximum once the arm is placed at half height of the body. It also shows a decreasing fluence rate once the arm is moved off centre, either in lower or higher position. Both these properties were already determined earlier as can be seen in figure 6.

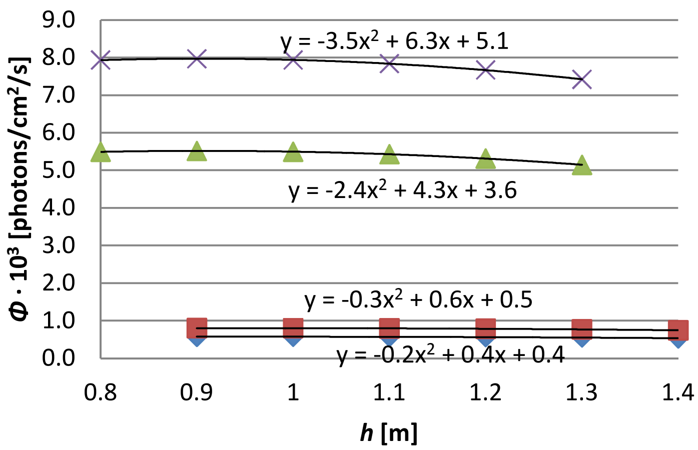

Figure 9. Graph that shows the fluence rate as a function of height for two arm positions. The blue and red line represent the fluence rates for photon energies of 113 keV and 208 keV respectively, for a sideways extended arm. The green and purple line the fluence rates for 113 keV and 208 keV photons respectively, for a forward extended arm.

Figure 10 illustrates the results of the simulations on the fluence rate for the two chosen arm positions. The fluence rate is, as in figure 9, greater for both 113 keV and 208 keV photon energies once the arm is extended forward. Ratios between both photon energies for the two arm positions can be found in table 7 located in appendix B2.

The figure also shows that the fluence rate is not decreased with the inverse square law. This is in accordance with the results presented in figure 8. Moreover, the power fit in figure 10 results in smaller powers for both photon energies than shown in figure 8, either with or without build-up.

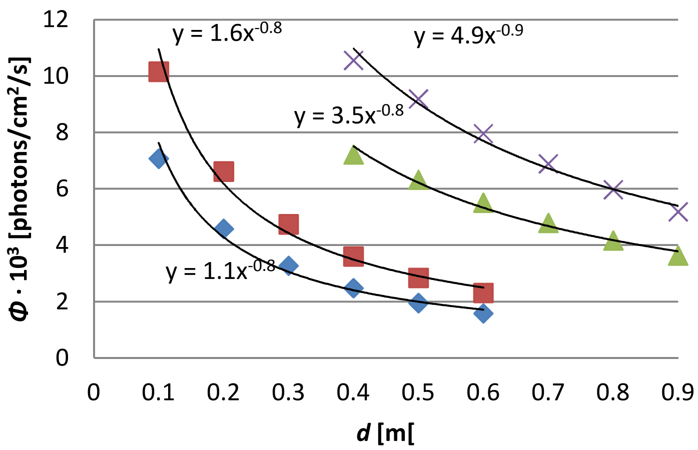

Figure 10. Graph that shows the fluence rate as a function of distance for two arm positions. The blue and red line represent the fluence rates for 113 keV and 208 keV photons respectively, for a sideways extended arm. The green and purple line the fluence rates for 113 keV and 208 keV photons respectively, for a forward extended arm.

From figure 9 and figure 10 it becomes clear that of the two arm positions, the better position is once the arm is extended sideways. In this arm position a lower fluence rate will be measurable. Thus, the optimized arm position is with the arm extended sideways. This can be explained when reviewing equation 22. This equation states that the photon fluence rate and concordantly the fluence rate depends on the area. The area is smaller of the geometry and body is smaller sideways than from the front.

However, optimized positioning of the detector system is patient specific. The length, height and thickness is different for each patient. Thus, making it impossible to optimize the position for all patient. Whilst this may be the case a standard position for the detector can be chosen taking into account that the measurable fluence rate will be lower when the detector and arm are position sideways. This standard position will be chosen rather arbitrarily. The position of the detector system will be set at 50 cm distance to the body at a height of 140 cm with respect to the body. Width position of the detector system will set for half patient thickness.

4.5. Conclusions

Results show that the fluence rate depends on two key parameters. For one, the geometry of the source. Second, the position with respect to the source. The geometry of the source will determine the isotropic or anisotropic nature of the fluence rate. An anisotropic property will lead to a position dependent fluence rate. In addition, the distance will also determine the measurable fluence rate.

Due to these position dependent photon fluencies an optimized arm position and detector position could be established. The optimized arm position proved to be a position in which the arm was extended sideways.

4.6. Discussion

It has been shown that a lower fluence rate will be measured once the detector is placed at wrist position with the arm extended sideways. However, optimizing the position to specific values proved more difficult. This is patient specific since arm lengths differ per patient. Though, it was possible to choose a standard position for the detector system. This standard position was set for a distance of 50 cm between the body and detector system, with the detector system placed at a height of 140 cm with respect to the body. The width position of the detector system was set for half of the bodies thickness.

In addition, the fluence rate will not be reduced sufficiently. Due to this the SNR will not be sufficient. Further reduction of the fluence rate can be achieved by shielding the detector system. Optimizations for shielding the detector system will have to be investigated.

5. Investigations on the signal-to-noise ratio.

5.1 Introduction & Objective

The level of noise, that is photons originating from the body instead of the wrist, can be reduced by optimal positioning of the detector system. However, optimized positioning of the detector system will not be enough to achieve a SNR of at least 100. Nevertheless, this SNR can still be achieved via several other possibilities. The aim is to determine the easiest and most efficient method to increase the SNR.

5.2 Problem description and solution

The detector system will be located around the forearm/wrist, and focused on blood vessels (arteries and veins). Photons originating from the blood within the field of view of the detector are regarded as signal (S). Photons originating from any other source like for example the rest of the body are regarded as background radiation. These photons will be counted and recorded as signal when in fact this is noise (N).

The levels of signal and noise can be described mathematically, albeit simplified, by multiplication of the amount of activity with the detector efficiency:

$$S = A_{bl} \cdot \varepsilon_{D_{bl}} \cdot \frac{1}{r^2} \tag{25}$$

$$N = A_{body} \cdot \varepsilon_{D_{body}} \cdot \frac{1}{R^2} \tag{26}$$

Where A_{bl} is the amount of activity in the blood [Bq], A_{body} is the amount of activity in the body [Bq], $\varepsilon_{d,bl}$ is the detector efficiency for the measurement of the amount of activity in the blood [-], $\varepsilon_{d,body}$ is the detector efficiency for the measurement of the amount of activity in the blood [-], r is the distance between arm and detectors [m] and R is the distance between body and the detector system [-].

The detector efficiency is assumed to be equal for both measurements thus can be removed from the equation. With equations 25 and 26 a formula for the SNR can be derived:

$$SNR = \frac{S}{N} = \frac{A_{bl}}{A_{body}} \cdot \frac{R^2}{r^2} \tag{27}$$

Since the detector efficiencies have been assumed to be equal, the SNR depends on the ratio between the amount of activities in blood and body and the ratio in the distances.

An efficient method of increasing the SNR is to reduce the noise. Reduction of noise can be achieved by minimizing the detectable amount of activity in the body and increasing the distance as can be seen in equation 27. It has also been shown that even with increased distance between the detector the level of noise

This minimization can be achieved by shielding the detectors from the activity in the body. In shielding the detectors there are certain criteria that will determine to what extent the noise can be reduced. These criteria are:

- Material used for shielding
- Thickness of the shielding
- Geometry (shape) of the shielding

Successfully reducing the number of photons, or fluence rate, can be achieved by using materials with high atom numbers (§2.1), such as lead or tungsten. Lead is preferred since it has a high attenuating property and its relatively cheap to obtain. In addition, it is a soft metal which makes it very malleable.

Thickness of the used shielding material will also determine to what extent reduction can be achieved. It may be clear that with increasing thickness the fluence rate or intensity will be reduced (§2.2). Thus the thicker the used material the lower the noise. However, increased thickness is accompanied by increased mass of the detector system. In addition, costs will be higher. Thus, an optimal thickness of shielding has to be determined.

5.3 Materials and methods

Determining level of Signal

The level of signal, that is the fluence rate at wrist position, is determined by simulations conducted with Microshield® . However, before these simulations could be conducted the amount of activity in blood of patients should be known. Data on the amount of activity in blood was collected from dr. Mark Konijnenberg at the Erasmus Medical Center. This data was published by Flavio Forrer et al.[3].

The data was analyzed by determining the average volume activity in blood for several points in time. Points in time that were considered are:

- t = 0 hours (immediately after infusion)
- t = 0,5 hours
- t = 1 hour
- t = 1,5 hours
- t = 24 hours
- t = 72 hours
- t = 96 hours
- t = 168 hours

The calculated volume activity for each moment in time was used to determine the fluence rates at detector position for both 113 keV and 208 keV photons. These fluence rates were determined by simulations that were conducted with Microshield® .

For these simulations a cylindrical geometry was created to simulate the forearm/wrist. This geometry consisted of 2 cylinders. One of these cylinders, the inner cylinder, represents the combined arteries and veins in the forearm and was given a radius of 0.22 cm. The other cylinder was placed around the first cylinder. This second cylinder was given a radius of 2.0 cm. Both cylinders were given a height of 7.2 cm. The combined length and diameter corresponds to a volume of 1 mL blood.

In the simulations the dose point, representing the detector, was placed at a height of 3.2 cm and a distance of 5.0 cm from the described geometry. The description of geometry and settings is shown in appendix C1.

Determining level of Noise

The level of noise is caused by the amount of activity in the remainder of the body, that is soft tissues, bone, organs and tumors. This level can be lowered by shielding the detector system from this activity. Simulations have been used to determine the level of noise at detector position for several thicknesses of shielding This was done by the thickness of shielding from 0.010 cm to 2.000 cm with increments of 0.105 cm.

In the simulation, the dose point (detector system) was placed at 50 cm distance at a height of 140 cm and at a width of 15 cm (half of the body width). Geometry of the body (rectangular volume) was identical to the geometry used in the previous chapter. Thus, the dimension used in the geometry were:

- Height: 1.80 m
- Length: 0.30 m (thickness)
- Width: 1.00 m

The fluence rate or noise was determined for two moments in time. First for the moment immediately after infusion (t=0) and second for 24 hours after infusion.

Improving SNR

The fluence rates for the level of signal and the level of noise were used to calculate the signal-to-noise ratio for several thicknesses of shielding. This was done for two important moments in time: t= 0 h and t = 24 h after infusion. Once the desired minimal SNR of 100 can be achieved for both these time points all measurements within 24 hours will have been performed with a SNR of 100.

5.4 Results

The amount of activity in the blood was determined for several points in time. This was done for 16 patients. The results for each patient was used to calculate the average amount of activity and according inaccuracy. This average amount of activity and inaccuracy are plotted in a graph. This graph can be seen in figure 11. The corresponding values can be found in table 8 in appendix C2.

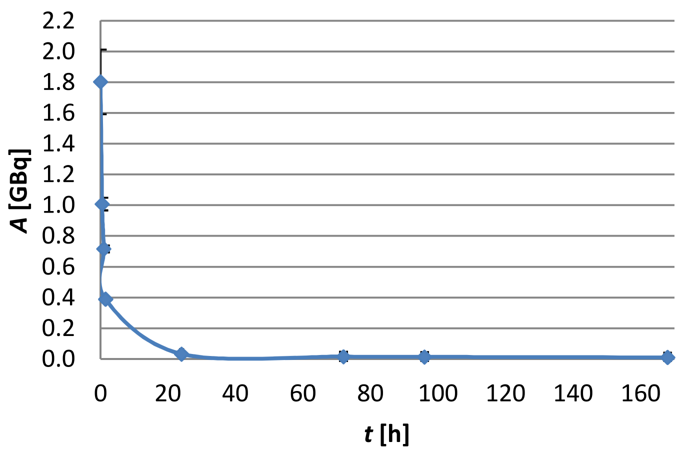

Figure 11. Graph that shows the average activity in blood of 16 patients as a function of time.

From figure 11 it can be seen that the amount of activity in the blood is rapidly decreased. In specific, the amount of activity is reduced to circa 1.7 % of the initial value within twenty-four hours.

The values for the amount of activity at several points in time were used in simulations to determine the fluence rate at detector position. This was done separately for the 113 keV and the 208 keV photons. The resulting detectable fluence rates were also plotted as a function of time, as can be seen in figure 12. Values used to plot the graph in figure 12 can be found in table 9 appendix C2.

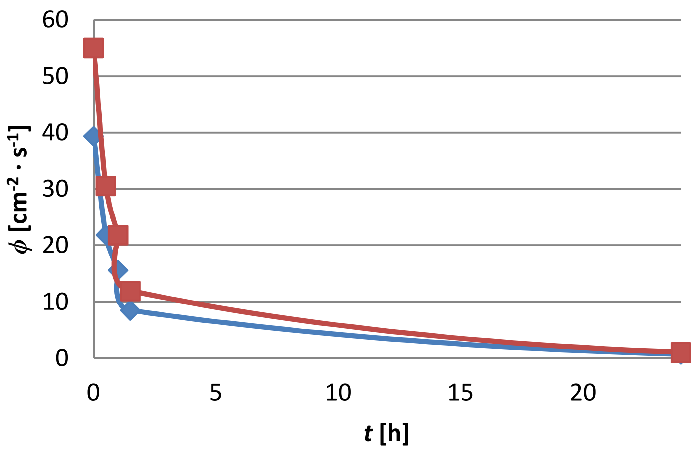

Figure 12. Graph that shows the detectable fluence rate as a function of time for 1 mL of blood at a distance of 5 cm. The average activity in 1mL of blood for 16 patients was used in this graph. The blue line represents the fluence rate of the 113 keV energy photons. The red line represents the fluence rate

In figure 12 only the fluence rates for the first 24 hours after infusion are shown. This is done because the detectable fluence rates have been decreased to an extent that makes external measurements rather difficult. As the fluence rate is decreased, the measurement time should be increased. However, long measurement times (more than 60 or 120 seconds) is not wanted. Thus, making measurements with the detector system longer than 24 hours after infusion impossible. Therefore, investigations on the SNR have been conducted for only two critical time points: 0 hours (immediately after infusion) and 24 hours after infusion.

The level of noise at detector position, that is fluence rate originating from the rest of the body, has been determined in presence of several thicknesses for the moment immediately after infusion. In addition, the same has been done for 24 hours after infusion. The results are shown in figure 13 and figure 14 respectively. The resulting values can also be found in tables 10 and 11 in appendix C2.

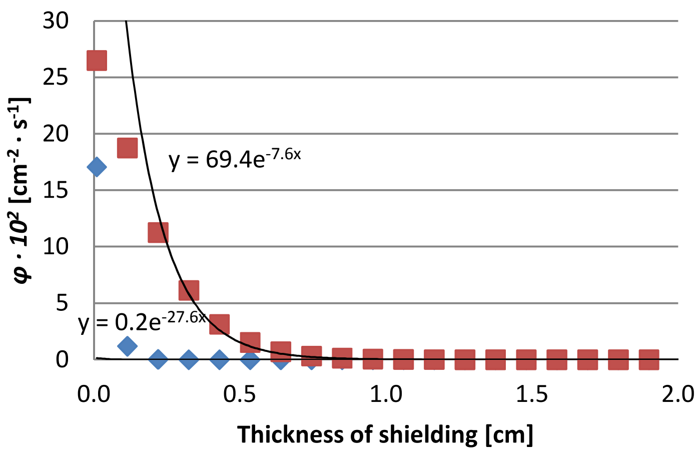

Figure 13. Graph in which the fluence rate is displayed as a function of the shielding thickness. In the graph the blue squares represents a photon energy of 113 keV. The red squares represent a photon energy of 208 keV

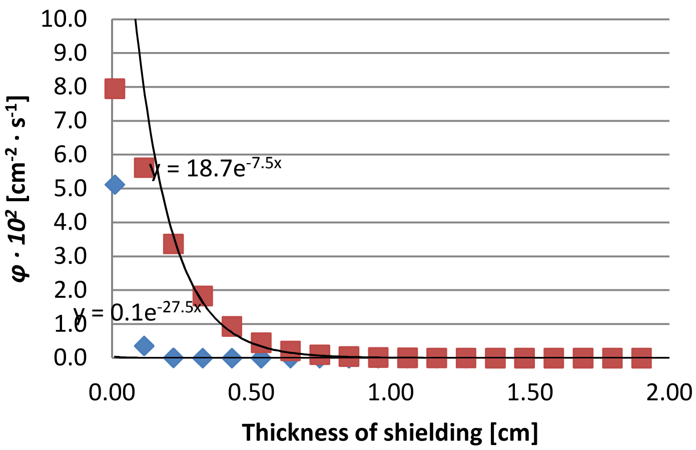

Figure 14. Graph that shows the fluence rate as a function of shielding thickness. In the graph the blue squares represents a photon energy of 113 keV. The red squares represent a photon energy of 208 keV.

In both figure 13 and figure 14 can be seen that the fluence rate is decreased exponentially, as expected. The value shown in the exponent of the equations represent the attenuation coefficient of lead for the specific energies in [cm^{-1}]. The values deviate from expected values, which are 52.5 [cm^{-1}] for 113 keV photons and 10.8 [cm^{-1}] for 208 keV photons[5]. The observed average values are 27.6 [cm^{-1}] for 113 keV photons and 7.6 [cm^{-1}] for 208 keV photons. The discrepancy in the values may be explained by the inaccuracy of the resulting fit as performed by Microsoft Excel. In addition, the geometry of the body causes a broad beam geometry for the photons. The attenuation coefficients are determined using a narrow beam geometry.

The levels of signal and noise for the time immediately after infusion and 24 hours after infusion have been used to calculate the signal-to-noise ratio. This was done for both 113 keV and 208 keV photon energies. In addition, the SNR was determined for multiple thicknesses of shielding. This showed that the signal-to-noise ratio increases rapidly as the thickness of shielding increases (level of noise is decreased as the thickness of shielding is increased). It also showed that the SNR increases less rapidly for 208 keV photons than for 113 keV photons. This is due to the difference in attenuation for photon energies. Thus, the SNR will be (mostly) determined by 208 keV photons and how well these photon can be stopped.

The relationship between the SNR and thickness of shielding can be clarified by a graph as is shown in figure 15. In this figure the logarithm of the SNR is displayed as a function of the shielding thickness. In the plot both t = 0 hours and t = 24 hours after infusion is shown.

[5] The mass attenuation coefficients have been determined by NIST and are published: http://physics.nist.gov/PhysRefData/XrayMassCoef/ElemTab/z82.html
Data from this table has been used to calculate the linear attenuation coefficient (data not shown)

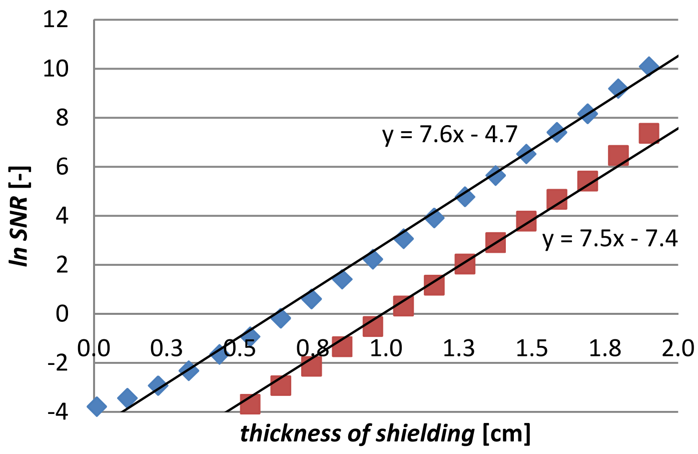

Figure 15. Graph that shows the SNR as a function of shielding thickness. The blue squares represent measurement immediately after infusion (t = 0 h). The red line represents measurements represent 24 hours p.i. (t = 24 h).

In figure 15 can be seen observed that the SNR is generally lower for 24 hours p.i. This can be explained by the shift in the level of signal and the level of noise as time progresses. The amount of activity in the blood is more rapidly decreased than the amount of activity in the body[6]. Equations in figure 15 can be used to calculate the thickness of shielding needed when a specific SNR is desired or required.

An error of 1% can be reached when the SNR is 100. A SNR of 100 can be achieved by using a thickness of 1.60 cm of lead shielding.

5.5 Conclusions

The amount of activity in the blood and in the body will determine the signal to noise ratio. It has been known that the amount of activity in the blood (circa 1.7 % of the injected amount) is decreased more rapidly than the amount of activity in the body (circa 30% of the injected amount). The difference in decrease of activity will result in a shift in the signal to noise ratio. Signal to noise ratios can be increased by lowering the noise which is achieved by using shielding.

Shielding the detector will cause a lowering of the level of noise or fluence rate. This fluence rate is reduced exponentially, as expected. The reduction of fluence rate differs for photon energies due to increasing stopping power for decreasing photon energies. As a consequence, highest photon energy should be used in calculating signal-to-noise ratios.

An error of 1% is obtained when a SNR of 100 is achieved. This SNR can easily be achieved by applying a specific thickness of shielding. However, the thickness needed to achieve a SNR of 100 is different for the moment immediately after (t = 0h) and 24 hours after infusion. For t=0 h 1.22 cm of lead shielding is adequate to achieve a SNR. For t = 24 hours at least 1.60 cm of lead shielding is needed.

5.6 Discussion

The level of noise is not solely determined by the amount of activity in the body. There is also a contribution by leakage of photons from outside of the field of view. In further investigations this contribution should be estimated or measured.

[6] The data is not shown but it is known that the amount of activity in the body, that is organs, tissue and tumors, is 30 ± 10 % of the injected dose.

6. Determination of detector properties

6.1 Introduction & objective

Measurements on the amount of activity in the blood need to be performed correctly, that is with a relatively small uncertainty. This is only possible if detector properties are known. Not all properties are known and therefore have to be determined. The aim is to determine the linearity of the detector and the detector efficiency for both detectors.

6.2 Problem

Linearity of the detector

Measurements on the amount of activity in blood can only be conducted correctly and accurately once detector properties are known. One of the important detector properties is the linearity. Linearity can be defined as the identical response of the detector on various amounts of activity.

During measurements on the linearity of a detector there are variables that can complicate measurements and calculations. One of these variables is the geometry of the source. A point source would be the preferred geometry during measurements. However, in practice point sources cannot be created. Sources will always have measurable dimensions. Luckily the influence of the geometry can be minimized.

Placing a source with relatively small dimensions at relatively large distance from the detector will create the opportunity to approximate the source as a point source. The source will then comply with the inverse squared law and the geometry can be easily included in all calculations. Thus making the following equation usable for calculations:

$$\phi = \frac{yA}{4\pi r^2} \tag{28}$$

Where φ is the fluence rate [$m^{-2} \cdot s^{-1}$], y is the abundance of the specific photon energy [-], A is the amount of activity [Bq] and is r the distance between source and detector [m]. This equation is used to determine activities needed for the linearity measurements (further described in materials & methods).

Detector efficiency

Another important property is the detector efficiency. This detector efficiency shows the ease with which the detector can measure radiation. It should be mentioned that this detector efficiency is energy dependent. In addition, like with measurements on linearity, measurements on the detector efficiency may be complicated by geometry of the source. By also using sources with small dimensions in comparison to the detector surface the sources can be approximated as point sources. With this specific condition met during measurement the following equation can be used to calculate the detector efficiency:

$$\varepsilon = \frac{\phi_m}{\phi_t} = \frac{R}{\frac{yA}{4\pi d^2}\pi {r_d}^2} = \frac{4Rd^2}{yA{r_d}^2} \tag{29}$$

Where ε is the detector efficiency [-], R is the measured rate [s^{-1}], d is the distance between source and detector [m], y is the yield or abundance for specific photon energies [-], A is the amount of activity and r_d is the radius of detector surface [m].

6.3 Methods & Materials

Each detector used for measurements consisted of a $CeBr_3$ scintillation crystal that was linked to a photomultiplier tube. This entire set-up was linked to a offsprey (Canberra) communication and power supply

Detector linearity

The average amount of activity in the blood for several point in time has already been determined and shown in chapter 5. In addition, the fluence rate at detector position for each point in time has already been determined by simulations. This fluence rate was used to calculate the amount of activity needed in a source of ^{177}Lu when the source was placed at 2 m distance from the detector. The results of the simulations and calculations are shown in tables 14 to 17 in appendix D3.

Measurements on the detector linearity are based on these activities and were included with additional activities. This was done to determine at what activity the linearity would be compromised. Eventually twelve different amounts of activity were measured in two different vials. In specific, seven of the twelve activities were measured in a volume of 10 mL in a vial of 10 mL. The remaining activities were measured in a volume of 100 mL in 100mL IV bottles. Measuring times were specifically chosen for each activity. The aim was that the counting error would be less than 1 %.

Each measurement was conducted three times to determine repeatability and make proper statistics possible. All measurements were conducted for the two detector simultaneously. This was possible due to the placement of the detectors with respect to each other. The detectors were placed opposite from each other with 4 m distance between the detectors.

Detector efficiency

The detector efficiency was determined for both detectors by measuring the amount of photons for different distances between the source and detector. During measurements, the measurement time was kept constant at 60 seconds. The measurements were conducted using two amounts of activities of ^{177}Lu in small volumes of 25 µL each.

Activities used were: circa 12.6 MBq and circa 22.7 MBq (exact values are presented later). The lower amount of activity was used in measurement in which the distance between the source and detector was varied from 7.0 to 13.0 cm. The higher amount of activity was used in measurements in which the distance was varied from 15.0 to 35.0 cm

6.4 Results

Detector linearity

The amount of detected photons were corrected for background radiation, and the total amount of disintegrations during the measurement time was calculated. Calculations were done with the equation presented in appendix D1. The results of measurements and calculations for each detector and each photon energy were collected and plotted in separate graphs including the inaccuracy of each measurement.

Detector 279

In figure 16 and figure 17 the results of the linearity measurements for the detector designated as 279 are shown. The corresponding values and inaccuracies can be found in tables 14 to 17 in appendix D3. Figure 16 shows the linearity plot for 113 keV photons.

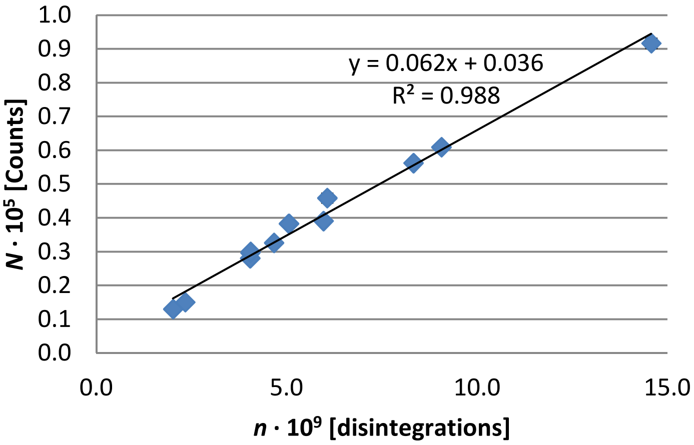

Figure 16. Graph in which the amount of detected 113 keV photons is displayed as a function of the number of disintegrations during the measurement time interval for detector 279.

The linearity of the detector is determined by applying linear regression theorem on both figure 16 and figure 17. This regression analysis showed that the detector is linear for the various amounts of activity used since the r proved to be 0.993. The response of detector proved to be (0.062 ± 0.002) count/disintegration for 113 keV photons.

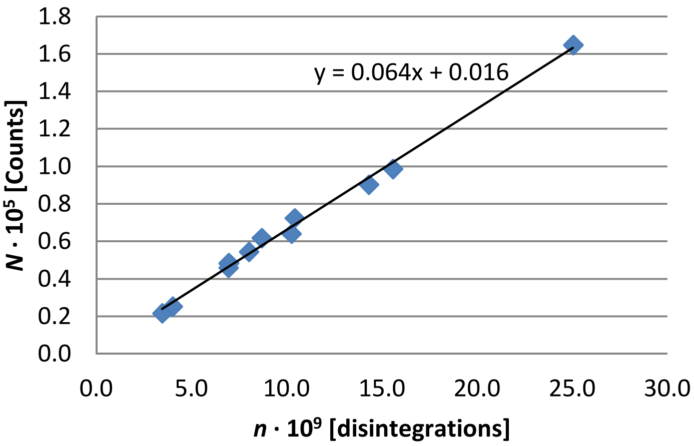

Figure 17. Graph in which the amount of detected 208 keV photons is displayed as a function of the number of desintegrations during the measurement time interval for detector 279.

The detector linearity for 208 keV was analyzed in a similar manner as for the 113 keV photons. Thus regression analysis was also performed on the values used for figure 17. This resulted in conformation of linearity of the detector for all amounts of activity used. And showed that the response of the detector for 208 keV photons is (0.064 ± 0.002) count/disintegrations.

These results show that the detector response is higher for 208 keV photons than for 113 keV photons albeit marginally higher. This suggests that detection for low energy photons is more difficult. A reasonable explanation could be that low energy photons might lose energy before they could excite atoms in the crystal and therefore less signal is produced. However, another reasonable explanation could be that the difference in response is within inaccuracy interval of the measurements.

Detector 276

The results of measurements for detector 279 were analyzed in a similar manner as was done for detector 276. Figures 18 and 19 show the measurement result for 113 keV and 208 keV photon energies respectively. All corresponding values including inaccuracies are presented in tables 18 to 21 in appendix D3.

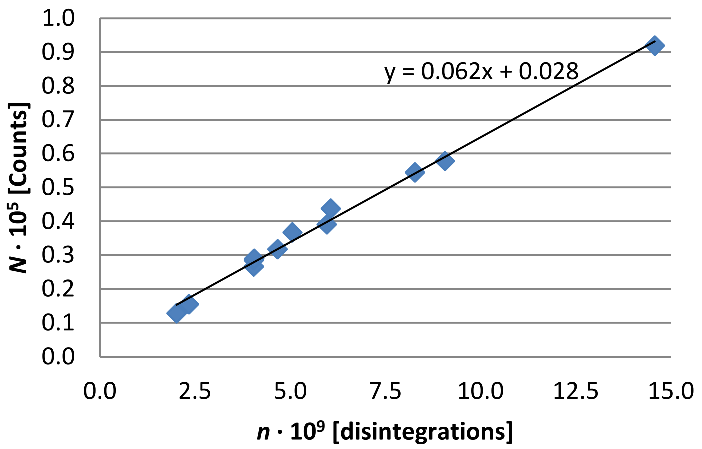

Figure 18. Graph in which the amount of detected 113 keV photons is displayed as a function of the number of desintegrations during the measurement time interval for detector 279.

Regression analysis on detector linearity for 113 keV and 208 keV was performed. This analysis resulted in a response of (0.062 ± 0.002) counts/disintegration for 113 keV and a response of (0.063 ± 0.002) counts/disintegration for 208 keV photons.

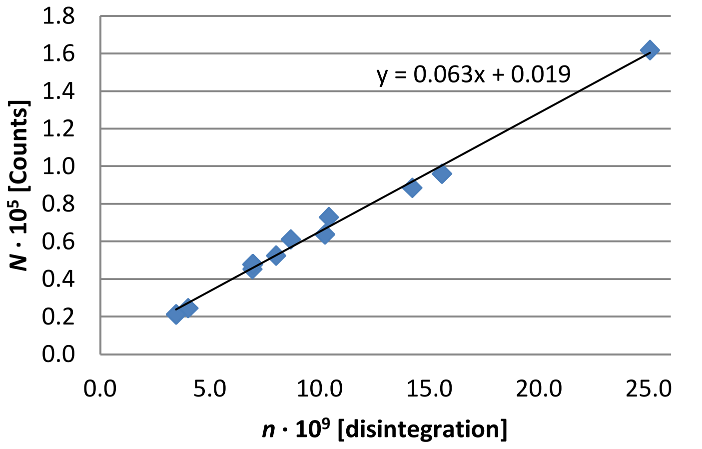

Figure 19. Graph in which the amount of detected 208 keV photons is displayed as a function of the number of desintegrations during the measurement time interval for detector 279.

These results in detector response also overlap and are closer together than for detector 279. This shows that the inaccuracy in measurements indeed are the responsible for the deviation in response for the two photon energies.

Detector efficiency

The number of photons detected were corrected for background radiation. Subsequently, the number of photons in each measurement were converted to rate. In addition, the theoretical rate was calculated. The detector efficiency could then be calculated using equation 29. The detector efficiency is plotted in a graph as function of the distance between the source and the detector. This type of graph will

Detector 279

In figure 20 the results are presented for 113 keV and 208 keV photon energies respectively. The inaccuracy in the measurements are included in the figure.

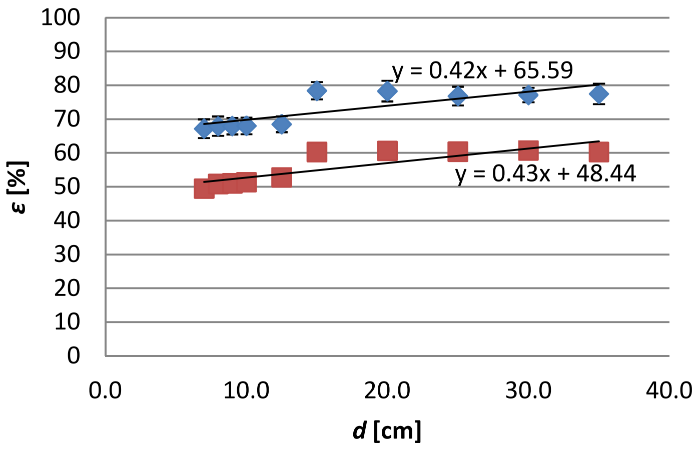

Figure 20. Graph in which the detector efficiency is plotted as a function of the distance between the source and detector. The blue line represents 113 keV energy photons and the red line 208 keV energy photons.

In figure 20 can be seen that the detector efficiency is increased as the distance between the source and the detector is increased. In addition, it can be seen that the detector efficiency depends on the photon energy. The same can be observed in figure 21. In figure 21 the results of measurements on detector 276 are presented.

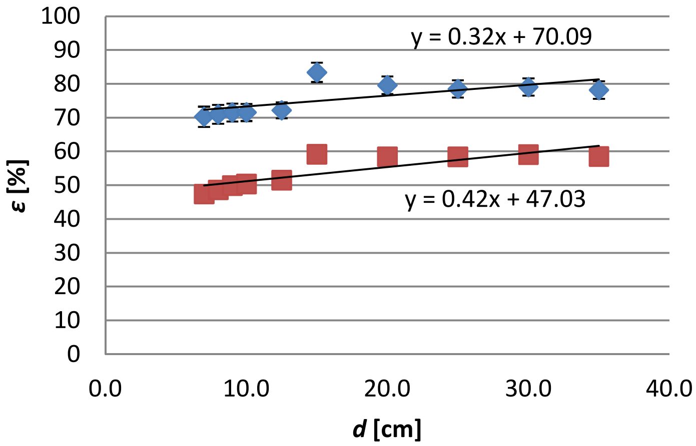

Figure 21. Graph in which the detector efficiency is plotted as a function of the distance between the source and detector. The blue line represents 113 keV energy photons and the red line 208 keV energy photons.

In both figure 20 and figure 21 it can be observed that the decrease in efficiency can be approximated with a power fit. And that this power fit approaches the inversed square law.

The equations from the fits create the opportunity to calculate the detector efficiency for a specific distance between source and detector. The source eventually being the arm. A known efficiency of the detector will make the estimation of the amount of activity in the blood possible.

6.5 Conclusions

Experiments show that both detectors are linear for activities ranging from 18 MBq to 4 GBq. It should be stated that the detectors are linear when these activities are placed at 2 m distance. This implies that the detector is linear within the range of activities in which measurements on the wrist/forearm wil

This can also be expressed as a response, and this response proved to be equal for both detectors. However, this is only the case for 113 keV photons. Photons energies of 208 keV show a similar but not equal response with the detectors. The response for 113 keV photons is (0.062 ± 0.002) counts/disintegration. For 208 keV photons the response is shown to be (0.063 ± 0.002) counts/disintegration and (0.064 ± 0.002) counts/disintegration for detector 276 and 279 respectively.

The detector efficiency has also been determined for both detectors, and for both 113 keV and 208 keV photon energies. The efficiencies for 113 keV photons proved to be (76 ± 5) % and (73 ± 6) % for detector 276 and detector 279 respectively. For 208 keV photons, the efficiencies proved to be (54 ± 5) % and (56 ± 5) % for detector 276 and detector 279 respectively.

6.6 Discussion

The detectors proved to be linear for a range of activities. The actual linearity of the detectors can only be determined once the response starts to deviate. Therefore, absolute linearity measurements of the detector demands that the range of activities is increased to the point that the response starts to deviate.

The detector efficiency was determined with a relatively large inaccuracy. This inaccuracy might have been caused by the use of two separate sources. Another explanation could be found in the solid angle during measurement. This solid angle is changed as the distance is increased. For larger distances the photons tend to enter the detector more parallel and almost perpendicular to the detector surface. The path length for photons then becomes practically equal and will only then give an accurate detector efficiency.

7. Investigations on optimal detector position with respect to the arm.

7.1 Introduction & objective

The total amount of activity in blood can be determined by measuring the volume activity of blood. This could be done by means of external measurements of the forearm. These external measurements would require correct and accurate determination of the volume of blood. The volume of blood is determined by the field of view of the detector. The field of view of the detector can be reduced by means of shielding. However, this would also reduce the amount activity that can be detected and will hereby influence the accuracy of the measurement. The aim is to determine the optimal position for detectors with respect to the arm in which accuracy during measurement is least affected.

7.2 Theoretical foundation

Measurements on the volume activity in blood can only be conducted once the volume of blood can be determined accurately. The measurable volume of blood is determined by the field of view of the detector. An unshielded detector can measure activity originating from any direction. In addition, an unshielded detector could not be used in measurements since the volume corresponding to the measured activity would be unknown. Thus, shielding (collimating) the detector will create the opportunity to determine the measurable volume of blood.

Although the field of view may be critical in determining the measurable volume of blood, it is not the only parameter in that has to be determined accurately. The geometry of the source, in this case the forearm, is another important parameter. The influence of the geometry should and can be minimized during measurements. This can be achieved by increasing the distance between source and detector. With increasing distance the source will approximate a point source geometry. A point source has in fact no measurable geometry. For point sources equation 28 can be used.

There is a disadvantage in increasing the distance between the source and detector. Increased distance will decrease the measurability of activity.

7.3 Methods and materials

Measurable number of photons as of function of sample length

Microshield® has been used to conduct simulations to determine the theoretical detectable fluence rate at detector position in case the detector is placed near the wrist/forearm. This determination has been done for two points in time. The points in time were moments immediately after and 24 hours after infusion. In the simulations the geometry of the forearm was regarded as a cylinder (as was done in §..). The dimensions of the geometry were equal to the dimensions used in paragraph 6.2. However, the simulation was conducted for three different sample lengths[7]:

- 7.2 cm
- 10.0 cm
- 12.5 cm

In each simulation the fluence rate was determined for several different distances between sample (forearm) and detector. The distances used were:

[7] The section of forearm as observed by the detector is defined as the sample. The sample length will then also represent a section of the arm with a specific length.

- 0.0 cm (detector placed on the skin)
- 2.0 cm
- 4.0 cm
- 6.0 cm
- 8.0 cm
- 10.0 cm

The resulting fluence rates were combined with the earlier determined detection efficiency to estimate (calculate) the number of detected photons after a measuring time of second seconds. This estimation has also been conducted for the two points in time, as mentioned earlier.

Theoretical field of view

The field of view has been determined for the parameters used in simulations on the measurable number of photons. In specific, the used parameters are the distance between the detector and source and the sample length.

Measurements on the field of view

Measurement have been conducted to determine whether it was possible to create a specific field of view by shielding the detectors. In the measurement a source of ^{177}Lu has been used. This source was created by placing a volume of less than 5 µL in a small vial (Mobitec). This vial then contained an activity of (2.2 ± 0.1) MBq.

This vial was placed opposite from the detector at a distance of 10 cm between source and detector. This detector was wrapped cylindrically in lead layer creating a shielding thickness of 1.5 cm. The detector was placed within the shielding in which the shielding extended 5.8 cm with respect to the detector.

In measurements the source was moved sideways along a straight line. This would create the change in angle between the detector centre and the source. This was done for circa 7.5 cm in both positive and negative direction. The positive direction was defined as being positions right to the center of the detector and the negative direction was defined as being positions left from the center of detector. The measuring time was kept constant at 60 seconds for each measurements.

7.4 Results

Measurable number of photons at detector position

The fluence rate at detector position has been determined for different sample lengths. The resulting fluence rate has been used to estimate the number of photons that will have been detected after 60 seconds of measurement. Simulations and estimations have been conducted for both the moment immediately and 24 hours after infusion, and 113 keV and 208 keV photon energies.. All results of simulations and estimations (calculations) have been collected and organized in tables 26 to 31 in appendix E2.

The results shown in the before mentioned tables has been plotted in graphs. However, only results for the 208 keV photons have been shown in the graphs. First, the results for the moment immediately after infusion are shown in figure 22.

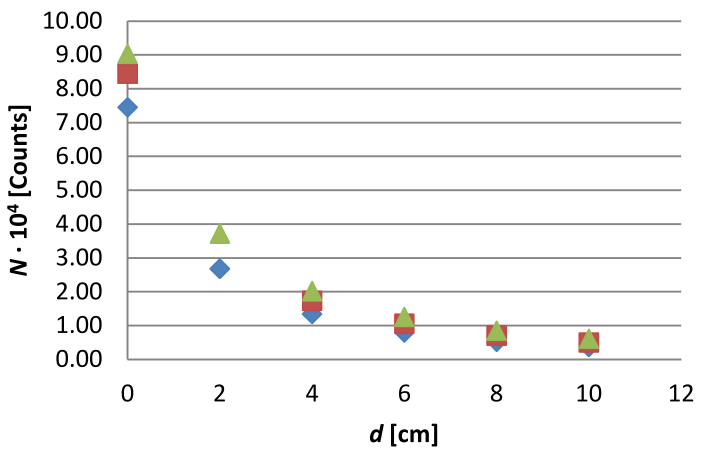

Figure 22. Graph in which the theoretical detectable number of 208 keV photons is plotted as a function of the distance between the source and detector for moment immediately after infusion (*t*=0 h). In the graph three lines are shown that each represent a different sample lengths. Blue, red and green represent 7.2 cm, 10 cm and 12.5 cm respectively.

From figure 22 can be observed that the estimated number of detected photons is higher for longer sample lengths. However, this is only for small distances between the sample and detector. Increasing the distance between sample and detector will result in a similar estimated number of detected photons.

Figure 22 can be used to determine the distance between source and detector when a specific number of detected photons is required. In addition, the figure can be used to chose a specific sample length. For the detector system purposes a minimum of 10000 counts is desired. This number of counts can be achieved when the distance between sample and detector is less than 6 cm, as can be seen in figure 22. However, a larger distance is desired. A larger distance and the desire for at least 10000 counts can also be reached by elongating the counting time to for example 120 second. It will then be possible to enlarge the distance between sample and detector to 10 cm.

As in figure 22, the estimated number of detected photons is plotted as function of distance between source and detector. However, in this plot the results are shown for simulations and estimations for 24 hours after infusion.

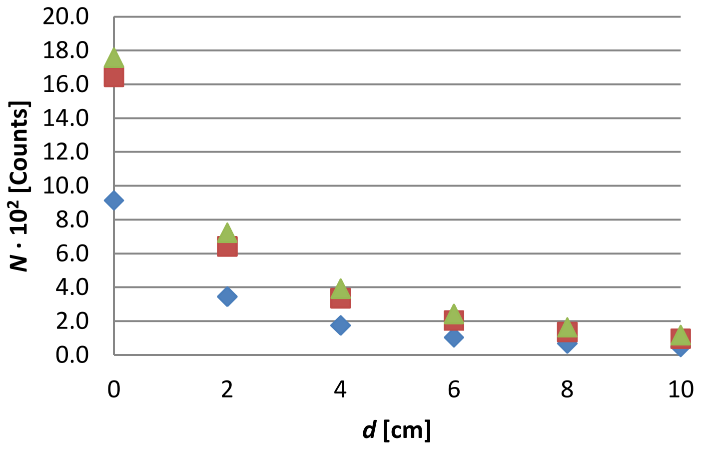

Figure 23. Graph in which the theoretical detectable number of 208 keV photons is plotted as a function of the distance between the source and detector. In the graph three lines are shown that each represent a different sample lengths. Blue, red and green represent 7.2 cm, 10 cm and 12.5 cm respectively.

In figure 23 can be seen that like in figure 22 the number of detected photons is decreased once the distance between source and detector is increased. However, in contrast to figure 22 the number of photons is reduced by a factor of approximately 50 to 100 depending on the distance. It can also be observed that the value of 10000 counts will not be reached by any distance. This value can only be reached by increasing measuring time 5 to 100 times the initial measuring time of 60 seconds. This depends on the distance between the detector and source.

Theoretical Fields of view

The measurable sample length is determined by the field of view. Each sample length and distance between sample and detector requires its own field of view. This theoretical field of view has been calculated and shown in table 32 of appendix E3

Determined Field of View

Experiments have been conducted to determine whether the FOV was easily adjustable by means of shielding. In addition, the experiments have been used to the determine the effects on the detected number of counts after narrowing the FOV. This has been done for each detector separately. Results for both detectors are shown in tables 33 to 36 in appendix E4

In figures 24 and 25 the results for both 113 keV and 208 keV photons are shown for detector 276 and 279 respectively. In each figure the number of detected photons has been plotted as a function of the angle between detector and sample. In both figures the inaccuracy in measurements has been shown. It should be stated that an angle of 0^o represents sample position directly opposite of the center of the detector.

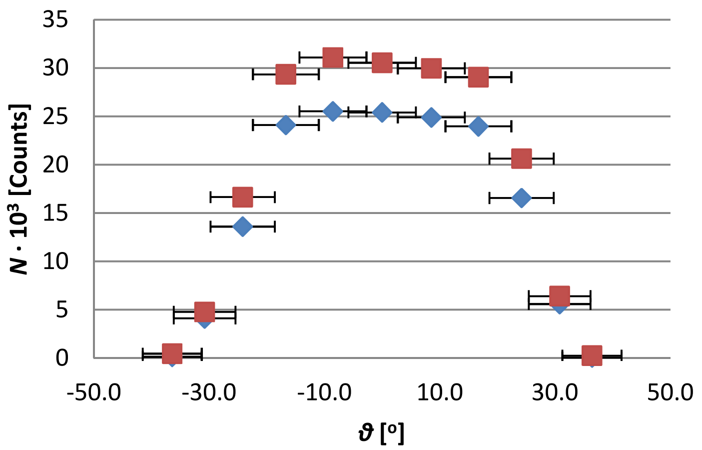

Figure 24. Graph in which the detected number of photons is plotted as a function of the angle between source and detector for detector 276. In this graph data on both 113 keV and 208 keV photons is plotted separately.

In figure 24 can be seen that the number of detected photons is practically similar for angles -17^{o} to 17^{o}. Beyond these angles, in both positive and negative directions, the number of detected photons is decreased rapidly. Beyond angles of -31^{o} and 31^{o} no photons, originating from the sample, will be detected. These effects can be explained by the shielding surrounding the detector.

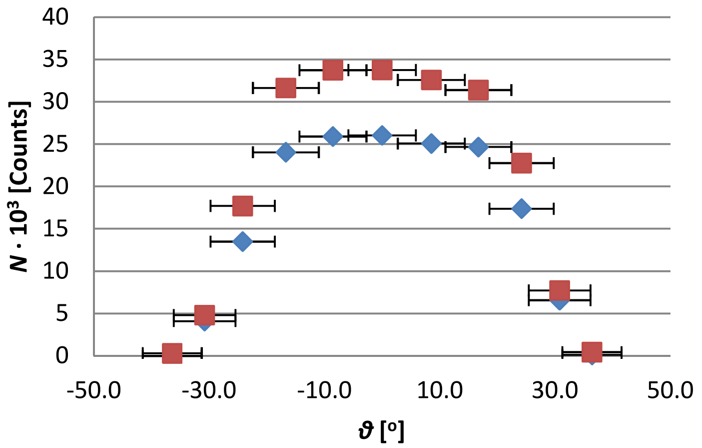

Figure 25. Graph in which the detected number of photons is plotted as a function of the angle between source and detector for detector 279. In this graph data on both 113 keV and 208 keV photons is plotted separately.

In figure 25 a similar curve can be observed as shown in figure 24. The values of angles are equal to the values mentioned with figure 24.

It should be mentioned that the slope of the decrease of number of detected photons can be altered by changing the shape (geometry) of the shielding (collimation). For correct sample length (volume of blood) measurements the slope should be as steep as possible. However, the number of detected photons should be similar for all angles within the field of view.

7.5 Conclusions

Simulation results confirm that the influence of the geometry is decreased as the distance between source (forearm) and detector is increased. Results show that for distances equal to and larger than 10 cm the will result in fluence rates that are similar independent from the sample length. It has also been shown that a minimal number of 10000 counts can be achieved within or after a measurement time of 60 seconds by positioning the detector at a maximum distance of 6 cm for the moment immediately after infusion. This number of counts cannot be achieved within or after measuring for 60 seconds.

For each distance the necessary field of view was calculated except for a distance of 0 cm. At this distance the detector surface would be in direct contact with the source (forearm) surface. It will then be impossible to create the large FOV necessary.

Results from experiments showed that it is possible to use lead shielding around the detectors (cylindrical in shape) to alter the field of view. The position of the detectors within the shielding will determine the field of view.

7.6 Discussion

Although the minimal number of 10000 counts cannot be achieved at t =24 hours with the set-up described in this chapter, the set-up might be altered/enhanced in a manner that this number can be achieved. For example, a detector with a larger size crystal can be used. Another possibility, however the less preferred possibility, is increasing measurement time.

Measurements on the FOV showed to have relatively large inaccuracies. These inaccuracies can be minimized by using a large distance than 10 cm in experiments. Displacement of the source, over the same distance as done in the experiments described in this chapter, will then result in a smaller change of the angle.

In addition, the slope in detected number of photons can be increased or decreased by changing the geometry of the shielding surrounding the detectors.

8. Project Conclusion

Investigations were conducted to determine whether a detector system could be developed that would be able to measure the amount of activity in blood. In these investigations several criteria were examined like positioning and signal to-noise ratio. In addition, detector properties were also examined. Properties like linearity, response and efficiency.

It has been reasoned that the detector system can be best positioned around an extremity. As a consequence, the distance between the body and the detector system can be increased. Subsequently, the detected number of photons originating from the body is reduced. For the best reduction the extremity should be extended out as far as possible creating the largest distance possible. The forearm/wrist was preferred of all extremities.

Moreover, it has been shown that the measurable fluence rate will differ for each arm position. It has also been shown that the best arm position is when the arm is extended sideways. This is defined as being the best position since the fluence rate of photons originating from the body is lowest at this position.

However, it has been determined that the fluence rate at this position is not reduced sufficiently. This will lead to an undesirable signal-to-noise ratio. Luckily, this SNR could be improved by the use of lead shielding. The thickness of shielding needed to achieve a SNR of at least 100 is 1.60 cm.

It became clear that theoretically it should be possible to determine the total amount of activity in the blood. Practically, this would only be possible once the before mentioned criteria were determined. These criteria have been determined and showed that the detectors are linear for a range of activities. This range of activities included the desired range of activities.

The response of the detectors proved to be equal for 113 keV photons with a value of (0.062 ± 0.002) counts/disintegration. In contrast to the response for 208 keV photons the detectors did not show an equal value. For 208 keV photons the response is (0.063 ± 0.002) counts/disintegration and (0.064 ± 0.002) counts/disintegration for detector 276 and 279 respectively.

The detector efficiencies were also determined. It was confirmed that the detector efficiency depends on photon energy. For detector 276 and 279 the efficiency proved to be (76 ± 5) % and (73 ± 6) % respectively for 113 keV photons. For 208 keV photons, the efficiencies proved to be (54 ± 5) % and (56 ± 5) % for detector 276 and detector 279 respectively.

Finally, the optimal detector position with respect to the arm were investigated. This investigation showed that at a distance of 10 cm between arm and detector the influence of geometry is minimized. There has also been shown that the field of view can easily be adjusted by applying shielding around the detector.

Now that all these criteria are determined further investigations can be conducted. These results do show that external measurements with this set-up should be feasible.

NB. All inaccuracies shown here have 1σ as degree of accuracy (68%). These inaccuracies can easily be calculated to a 3σ degree of accuracy (99.7%). This applies to the entire report.

9. Recommendations

Further investigations are needed to create a detector system that will be able to measure the amount of activity in blood with the highest accuracy possible. For one, the collimation needs to be designed correctly to reduce leakage of photons that originate from outside of the field of view. This can be done theoretically. Another possibility is to empirically determine the optimal geometry of the collimating shielding.

Once the correct collimation has been designed the following subjects can be investigated.

- Phantom measurements
- Level of attenuation of the wrist/forearm
- Patient measurements

Phantom measurements could be conducted by making a cylinder of Plexiglas in which a small tubing with a specific amount of activity is placed, and filling the cylinder with water. This experiments could be extended by placing actual bone in the Plexiglas cylinder and even adding more tubing to represent more arteries and veins.

These phantom measurements could be used to estimate the attenuation of the activity. However, the attenuation of the forearm could also be determined by means of a CT scanner. A patients arm can be scanned and the data can be used to determine the attenuation of each specific tissue[8].

Finally, the detector system should be used on patients to examine whether the amount of activity in blood of patients can be determined accurately. This will be done by taking blood samples and linking this the results of the blood sample to the measurement with the detector system.

[8] This data may already be available for a number of patients.

10. References

10.1 Articles

[1] Kwekkeboom DJ, Teunissen JJ, Bakker WH, Kooij PP, de Herder WW, Feelders RA, van Eijck CH, Esser JP, Kam BL & Krenning EP. Radiolabeled somatostatin analog [^{177}Lu-DOTA^{0},Tyr^{3}]octreotate in patients with endocrine gastroenteropancreatic tumors. Journal of Clinical Oncology (2005) 23 2754–2762.

[2] Esther I. van Vliet, Jaap J.M. Teunissen, Boen L.R. Kam, Marion de Jong, Eric P. Krenning Dik J. Kwekkeboom. Treatment of Gastroenteropancreatic Neuroendocrine Tumors with Peptide Receptor Radionuclide Therapy. Neuroendocrinology (2012)

[3] Flavio Forrer, Eric P. Krenning, Peter P. Kooij, Bert F. Bernard, Mark Konijnenberg, Willem H. Bakker, Jaap J. M. Teunissen, Marion de Jong, Kirsten van Lom and Wouter W. de Herder, et al. Bone marrow dosimetry in peptide receptor radionuclide therapy with [^{177}Lu-DOTA^{0},Tyr^{3}]octreotate. Eur J Nucl Med Mol Imaging (2009) 36:1138–1146

[4] Tran Quoc Dung, Nguyen Duc Thanh, Luu Anh Tuyen, Lo Thai Son, Phan Trong Phuc. Evaluation of a gamma technique for the assay of radioactive waste drums using two measurements from opposing directions. Applied radiation and Isotopes 67 (2009): 164-169.

[5] R.H. Pratt, Akiva Ron, H.K.Tseng. Atomic Photoelectric effect above 10 keV. Reviews of Modern Physics Vol 45, Number 2:273-322

[6] G. Breit. A correspondence principle in the Compton effect. Physical Review (1926)

[7] J.H. Hubbell. Electron-positron pair production by photons: A historical overview. Radiation Physics and Chemistry 75 (2006): 614-623

[8] Charlotte Meaker Davisson and Robley D. Evans. Gamma-Ray Absorption Coefficients. Reviews of Modern Physics Vol 24, number 2 (1952)

[9] P.Bode, M de Bruin, P.J.M. Korthoven. A method for the correction of self-absorption of low energy photons for use in routine INAA. Journal of radioanalytical chemistry (1982) Vol.64. No. 1-2:153-166.

[] Ashraf T, Panhwar Z, Habib S, Memon MA, Samsi F, Arif J. Size of radial and ulnar artery in local population. J Pak Med Assoc 2010 Oct;60(10):817-9

[] Kanai S. Shah, Jaroslaw Glodo, William Higgins, Edgar V.D. van Loef, William W. Moses, Stephen E. Derenzo, Marvin J. Weber. CeBr3 Scintillators for gamma-ray spectroscopy.

10.2 Books

A.J.J. Bos, F.S. Draaisma, W.J.C. Okx. Inleiding tot de stralingshygiëne. SDU uitgevers. ISBN:9789012382120

11. Appendices

Appendix A: Project description

Wrist measurement for determining activity in the blood

Background

Radionuclides therapies are treated in the department of nuclear medicine of EMC. A project of measuring directly the radioactivity in the excreted urine in toilet pot is being investigated by RIH, cooperating with EMC. Meanwhile, the whole body counting method has being investigated as well, accompanying with the urine collection method. The radioactivity in whole body could be determined by the urine measurement or whole body counting.

Objectives

Bone marrow is the most radiosensitive tissue in the body and it is commonly the dose-limiting tissue for radionuclide therapy. The dose to bone marrow is needed for the patient individual dosimetry. The activity in bone marrow is related closely with the activity in blood. Based on the activity in blood, the dose to bone marrow could be determined in addition with the activity in whole body.

Generally the activity in blood is determined by taking the blood samples at a given timeline after infusion. Taking blood samples frequently is boring for patients, and also leaves a radiation risk for the staff who handles the activity measurements of blood samples. Thereby it is needed to measure the activity in blood without taking the blood samples. Can the activity in blood be determined by measuring activity in the wrist?

Target

The target is to reduce the frequency of taking blood samples so that it is much comfortable for patients, and also reduce the radiation risk for the staff.

There are 8 treats per week. The frequency of taking blood samples is about 4 times with 24 h after infusion at least. When the project is completed, the one blood sample is needed still for the baseline measurement.

Activities/Study design

The radioactivity in wrist could be measured with a wrist measurement under a proper shielding against activity in the whole body. A well detector, which the diameter of the well volume should be suitable to wrist and hand size, could be used. For instance, a pressurized ionization chamber in dose calibrator VDC 505 or a well NaI detector could be a good choice. Alternatively, two scintillation detectors (cylinder) could be put on the opposite sides around the wrist.

Modeling

In order to optimize the setup of the wrist measurement, a simulation model will be developed by using the MNCP5 code or MicroShielding code. The model of the wrist consists of normal tissue, blood vessel and bone with different radioactivity levels. The distance between detectors and wrist should be optimized so that the impacts caused by the geometrical variations of the patient wrists could be minimized.

Phantom experiments

The simulation will be validated by the typical experiment with an arm phantom. The simple arm phantom could consist of a plastic cylinder filled with water which simulates normal tissue in arm, inserting a plastic tube which simulates vessels and blood in it. The radioactivity in normal tissue and blood could be changed by the ^{177}Lu activity in the cylinder and vessel tubes.

Patient measurements

At first the wrist measurements will be carried out at a given timeline for a few patients, accompanying with the blood samples. The ratio of the count rate of wrist measurement to the activity in the blood sample at t=0 h is used as the factor of the patient individual calibration. It may vary with time. A proper correction is needed for the variations of the ratios at other times.

$$R(t) = \frac{n(t)}{A^{s}{}_{b}(t)}$$

Where, n(t) is the count rate (cps) of the wrist measurement at time t, $A_b^s(t)$ is the activity (MBq/mL) in the blood sample, R(t) is the response.

For the normal wrist measurement, a blood sample will be taken immediately after infusion, which is used as the reference value of the patient individual calibration. The baseline wrist measurement at t=0 h can be used as the calibrations individually. Then the activities in blood can be determined by the count rates of the wrist measurements with the correction factors at other times.

$$A_b(t) = \frac{n(t)}{R(0)} f(t)$$

Where, $A_b(t)$ is the activity (MBq/mL) in blood, R(0) is the calibration factor and the f(t) is the correction factor.

Data analysis

The measurement uncertainty of the activity in blood will depend mainly on the variations of the ratio with time. The activity in wrist consists of three parts, e.g. activity in blood, normal tissue in wrist and bone (including bone and marrow in the bone in wrist). The activities in normal tissue and bone could come from the gamma camera scanning at t=24 h only. The time-activity curves in the different organs, e.g. blood, normal tissue and bone of the wrist are different for different patients.

Planning

Research schedule:

Modeling: March-May 2012

Phantom experiments: June-September 2012

Patient measurements: October - December 2012

Summarize: January 2013

Research group

The research group consists of the experts from TU Delft and EMC Rotterdam. They are:

TU Delft: Peter Bode, Boxue Liu (fulltime), Folkert D.P. Geurink, students (probably)

EMC Rotterdam: Wout Breeman, Mark Konijnenberg

Result publication/PR and Communication

The results will be presented in the annual conference of European Association of Nuclear Medicine and probably in a proper technical journal.

Appendix B1: Simulated geometries

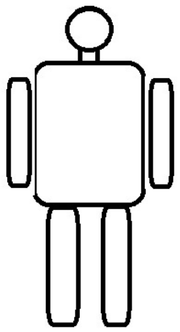

Figure 26. Schematic representation of the body in which the arms are position alongside the body. This representation has been used to determine the geometry used in simulations.

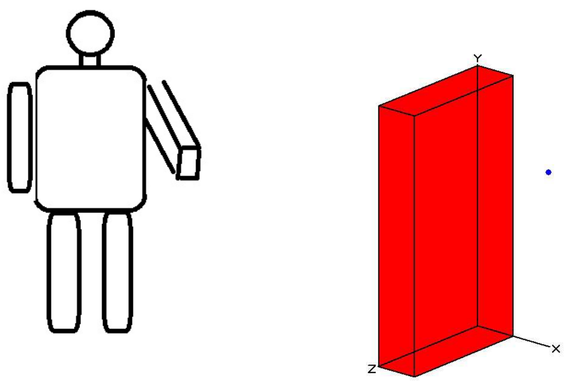

Figure 27. Schematic representation of the body and the corresponding geometry used to simulate the fluence rate of photons originating from the body at detector position where the arm would be extended forward.

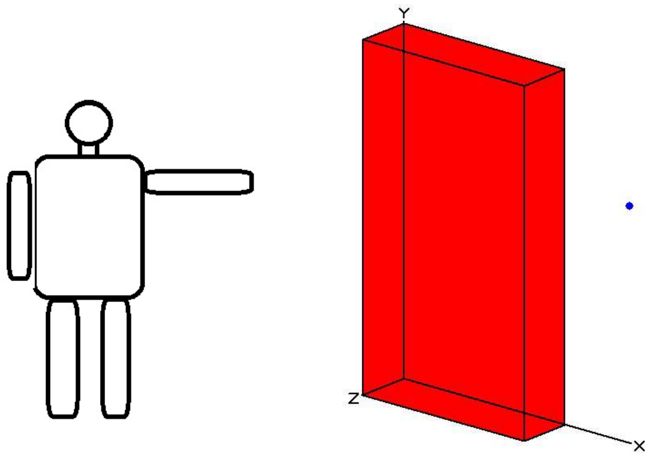

Figure 28. Schematic representation of the body and the corresponding geometry used to simulate the fluence rate of photons originating from the body at detector position where the arm would be extended sideways.

Appendix B2: Tables regarding position dependent fluence rates

Table 1. Results of the simulations on height dependent fluence rates

	without build-up	with build-up	without build-up	with build-up
E [KeV]	113	113	208	208
h [m]	$\varphi \cdot 10^3$ [$cm^{-2} \cdot s^{-1}$]	$\varphi \cdot 10^3$ [$cm^{-2} \cdot s^{-1}$]	$\varphi \cdot 10^3$ [$cm^{-2} \cdot s^{-1}$]	$\varphi \cdot 10^3$ [$cm^{-2} \cdot s^{-1}$]
0,7	1,53	8,38	3,13	12,0
0,8	1,54	8,48	3,16	12,1
0,9	1,54	8,51	3,16	12,1
1	1,54	8,48	3,16	12,1
1,1	1,53	8,38	3,13	12,0
1,2	1,50	8,22	3,08	11,7

Table 2. Results of the simulations on width dependent fluence rates

	without build up	with build-up	without build up	with build-up
E [keV]	113	113	208	208
w [m]	$\varphi \cdot 10^3$ [$cm^{-2} \cdot s^{-1}$]	$\varphi \cdot 10^3$ [$cm^{-2} \cdot s^{-1}$]	$\varphi \cdot 10^3$ [$cm^{-2} \cdot s^{-1}$]	$\varphi \cdot 10^3$ [$cm^{-2} \cdot s^{-1}$]
0,30	1,45	8,0	2,98	11,4
0,40	1,52	8,4	3,12	12,0
0,50	1,54	8,5	3,16	12,1
0,60	1,52	8,4	3,12	12,0
0,70	1,45	8,0	2,98	11,4
0,80	1,33	7,4	2,73	10,6

Table 3. Results of the simulations on distance dependent fluence rates

	without build up	with build-up	without build up	with build-up
E [keV]	113	113	208	208
d [m]	$\varphi \cdot 10^3$ [$cm^{-2} \cdot s^{-1}$]	$\varphi \cdot 10^3$ [$cm^{-2} \cdot s^{-1}$]	$\varphi \cdot 10^3$ [$cm^{-2} \cdot s^{-1}$]	$\varphi \cdot 10^3$ [$cm^{-2} \cdot s^{-1}$]
0,4	2,26	13,5	4,67	19,9
0,5	1,87	10,9	3,84	15,8
0,6	1,54	8,8	3,16	12,7
0,7	1,28	7,2	2,61	10,4
0,8	1,06	5,9	2,18	8,5
0,9	0,89	4,9	1,82	7,1

Appendix B3: Tables regarding the arm position dependent photon fluencies

Table 4. Results on the height dependent fluence rate for two arm positions.

arm sideways			arm forward		
E [keV]	113	208	*E* [keV]	113	208
h [m]	$\varphi \cdot 10^3$ [cm$^{-2}\cdot$ s^{-1}]	$\varphi \cdot 10^3$ [cm$^{-2}\cdot$ s^{-1}]	*h* [m]	$\varphi \cdot 10^3$ [cm$^{-2}\cdot$ s^{-1}]	$\varphi \cdot 10^3$ [cm$^{-2}\cdot$ s^{-1}]]
0,9	0,58	0,80	0,8	5,49	7,93
1	0,57	0,80	0,9	5,52	7,97
1,1	0,57	0,80	1	5,49	7,93
1,2	0,56	0,79	1,1	5,43	7,84
1,3	0,55	0,77	1,2	5,32	7,67
1,4	0,53	0,75	1,3	5,15	7,42

Table 5. Ratios between arm positions for both photon energies (height dependent)

h [m]	Ratio arm forward/arm sideways 113 keV photons	Ratio arm forward/arm sideways 208 keV photons
0,9	9,59	9,93
1,0	9,57	9,91
1,1	9,51	9,85
1,2	9,43	9,75
1,3	9,31	9,62

Table 6. Results on the distance dependent fluence rate for two arm positions.

arm sideways			arm forward		
E [keV]	113	208	*E* [keV]	113	208
d [m]	$\varphi \cdot 10^3$ [cm$^{-2}\cdot$ s^{-1}]	$\varphi \cdot 10^3$ [cm$^{-2}\cdot$ s^{-1}]	*d* [m]	$\varphi \cdot 10^3$ [cm$^{-2}\cdot$ s^{-1}]	$\varphi \cdot 10^3$ [cm$^{-2}\cdot$ s^{-1}]
0,1	7,1	10,2	0,4	7,2	10,6
0,2	4,6	6,6	0,5	6,3	9,2
0,3	3,3	4,7	0,6	5,5	8,0
0,4	2,5	3,6	0,7	4,8	6,9
0,5	2,0	2,8	0,8	4,2	6,0
0,6	1,6	2,3	0,9	3,6	5,2

Table 7. Ratios between arm positions for both photon energies (distance dependent)

d [m]	Ratio arm forward/arm sideways 113 keV photons	Ratio arm forward/arm sideways 208 keV photons
0,4	2,91	2,93
0,5	3,23	3,23
0,6	3,48	3,45

Appendix C1: Simulated geometry of the wrist.

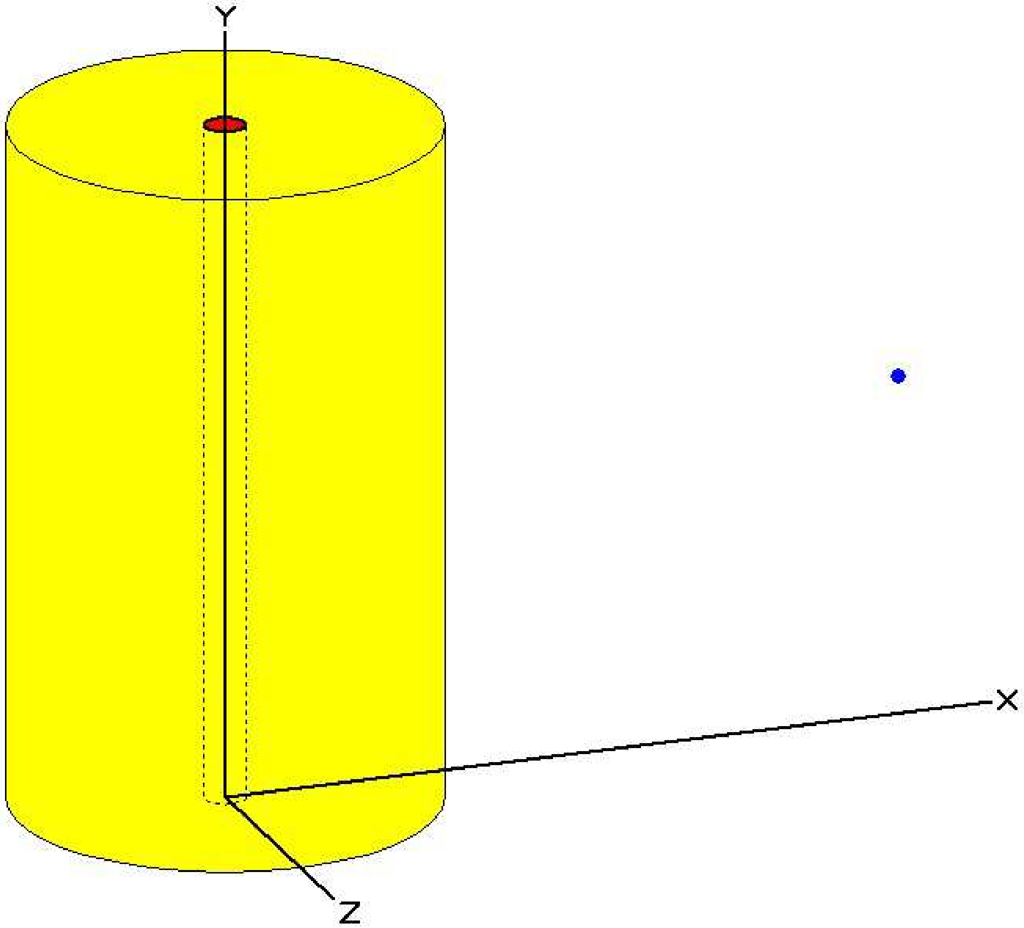

Figure 29. Geometry used to represent the forearm/wrist in simulations on the fluence rate at detector position.

Appendix C2: Calculations corresponding to wrist simulations

Determining the volume:

$$V = \pi r^2 l \tag{30}$$

Determining the combined radius of the geometry for simulation purposes:

$$V_{total} = V_1 + V_2 + V_3 + V_4 \tag{31}$$

$$V_{total} = \pi {r_1}^2 l + \pi {r_2}^2 l + \pi {r_3}^2 l + \pi {r_4}^2 l = \pi l \left({r_1}^2 + {r_2}^2 + {r_3}^2 + {r_4}^2\right) = \pi l R^2 \tag{32}$$

$$R = \sqrt{\frac{V_{total}}{\pi l}} \tag{33}$$

Determining the length of the geometry for simulation purposes:

$$l = \frac{V_{total}}{\pi R^2} \tag{34}$$

Appendix C3: Tables on the amount of activity in blood and fluence rates

Table 8. Average amount of activity in the blood of patients (n=16).

t [h]	*Δt* [h]	*A* [GBq]	*ΔA* [GBq]	$A \cdot 10^5$ [Bq/mL]	$\Delta A \cdot 10^5$ [Bq/mL]
0,0	0,03	1,80	0,21	3,61	0,42
0,5	0,03	1,01	0,04	2,02	0,08
1,0	0,08	0,72	0,02	1,44	0,04
1,5	0,17	0,39	0,01	0,78	0,02
24,0	0,50	0,03	0,00	0,07	0,00
72,0	1,00	0,02	0,00	0,03	0,00
96,0	1,00	0,02	0,00	0,03	0,00
168,0	1,00	0,01	0,00	0,02	0,00

Table 9. Results of simulations on the fluence rate emitted from 1 mL of blood in the wrist.

E [keV]	113	208
t [h]	φ [$cm^{-2} \cdot s^{-1}$]	φ [$cm^{-2} \cdot s^{-1}$]
0,0	39	55
0,5	22	31
1,0	16	22
1,5	8,5	11
24,0	0,74	1,0
72,0	0,37	0,52
96,0	0,33	0,46
168,0	0,25	0,35

Table 10. Results of simulations on the fluence rate (noise) in presence of different thicknesses of shielding (t = 0 h) .

E [keV]	113	208
shielding thickness [cm]	$\varphi \cdot 10^2$ [cm^{-2}/s^{-1}]	$\varphi \cdot 10^2$ [cm^{-2}/s^{-1}]
0.01	17.1	26.5
0.12	1.2	18.8
0.22	0.0	11.3
0.33	0.0	6.1
0.43	0.0	3.1
0.54	0.0	1.5
0.64	0.0	0.7
0.75	0.0	0.3
0.85	0.0	0.1
0.96	0.0	0.1
1.06	0.0	0.0
1.17	0.0	0.0
1.27	0.0	0.0
1.38	0.0	0.0
1.48	0.0	0.0
1.59	0.0	0.0
1.69	0.0	0.0
1.80	0.0	0.0
1.90	0.0	0.0
2.01	0.0	0.0

Table 11. Results of simulations on the fluence rate (noise) in presence of different thicknesses of shielding (t = 24 h)

E [keV]	113	208
shielding thickness [cm]	$\varphi \cdot 10^2$ [cm^{-2}/s^{-1}]	$\varphi \cdot 10^2$ [cm^{-2}/s^{-1}]
0.01	5.1	7.9
0.12	0.4	5.6
0.22	0.0	3.4
0.33	0.0	1.8
0.43	0.0	0.9
0.54	0.0	0.5
0.64	0.0	0.2
0.75	0.0	0.1
0.85	0.0	0.0
0.96	0.0	0.0
1.06	0.0	0.0
1.17	0.0	0.0
1.27	0.0	0.0
1.38	0.0	0.0
1.48	0.0	0.0
1.59	0.0	0.0
1.69	0.0	0.0
1.80	0.0	0.0
1.90	0.0	0.0
2.01	0.0	0.0

Table 12. Table on the relationship between shielding thickness and SNR.

t [h]	0	24
E [keV]	208	208
Shielding thickness **[cm]**	***Ln SNR*** **[-]**	***Ln SNR*****[-]**
0.0	-4	-2
0.1	-3	-2
0.2	-3	-1
0.3	-2	0
0.4	-2	0
0.5	-1	1
0.6	0	2
0.7	1	2
0.9	1	3
1.0	2	4
1.1	3	5
1.2	4	6
1.3	5	7
1.4	6	8
1.5	7	8
1.6	7	9
1.7	8	10
1.8	9	11
1.9	10	12
2.0	11	12

Appendix D1: Calculations for detector properties

Calculating the number of disintegrations during measurement time:

$$n = \int_0^T A_0 e^{-\lambda t} dt = \frac{A_0}{\lambda}\left(1 - e^{-\lambda T}\right) \tag{31}$$

Where n is the number of disintegrations [-], A_0 is the amount of activity at start measurement [Bq], λ is the decay constant of the radionuclide [s^{-1}] and T is the measurement time [s].

Calculating the response of the detector:

$$R = \frac{N}{n} \tag{35}$$

Calculations on the uncertainty

Calculating the uncertainty in the number of detected photons:

$$\Delta N = \frac{s}{\sqrt{n}} \tag{36}$$

Where ΔN is the uncertainty in the number of detected photons [Counts], s is the standard deviation in the measurement [Counts] and n is the number of measurements[-].

Calculating the uncertainty in the number of disintegrations:

$$\Delta n = \left|\frac{dn}{dA_0}\right| \cdot \Delta A_0 \tag{37}$$

$$\Delta n = \left|\frac{1}{\lambda}\left(1 - e^{-\lambda T}\right)\right| \cdot \Delta A_0 \tag{38}$$

Where Δn is the uncertainty in the number of disintegrations [-], ΔA_0 is the uncertainty in the amount of activity at start measurement [Bq], λ is the decay constant of the radionuclide [s^{-1}] and T is the measurement time [s].

Calculating the uncertainty in the response of the detector:

$$\Delta R = \left|\frac{dR}{dN}\right| \cdot \Delta N + \left|\frac{dR}{dn}\right| \cdot \Delta n \tag{39}$$

$$\Delta R = \left|\frac{1}{n}\right| \cdot \Delta N + \left|-\frac{N}{n^2}\right| \cdot \Delta n \tag{40}$$

Calculating the uncertainty in the detector efficiency:

$$\varepsilon = \frac{4Rd^2}{yA{r_d}^2} \tag{41}$$

$$\Delta\varepsilon = \left|\frac{d\varepsilon}{dR}\right| \cdot \Delta R + \left|\frac{d\varepsilon}{dd}\right| \cdot \Delta d + \left|\frac{d\varepsilon}{dA}\right| \cdot \Delta A + \left|\frac{d\varepsilon}{dr_d}\right| \cdot \Delta r_d \tag{42}$$

$$\Delta\varepsilon = \left|\frac{4d^2}{yA\,{r_d}^2}\right| \cdot \Delta R + \left|\frac{8Rd}{yA{r_d}^2}\right| \cdot \Delta d + \left|-\frac{4Rd^2}{yA^2{r_d}^2}\right| \cdot \Delta A + \left|-\frac{4Rd^2}{2yA{r_d}^3}\right| \cdot \Delta r_d \tag{43}$$

Appendix D2: Theoretical fluence rates for linearity measurement

Table 13. The simulated fluence rates and the corresponding amount of activities needed to measure these fluence rates at 2 m distance.

E [keV]	113	208	113	208
t [h]	φ [$cm^{-2}\cdot s^{-1}$]	φ[$cm^{-2}\cdot s^{-1}$]	$A \cdot 10^2$ [MBq]	$A \cdot 10^2$ [MBq]
0.0	42	61	3.3	2.8
0.5	23	34	1.8	1.6
1.0	17	24	1.3	1.1
1.5	9.0	13.2	0.71	0.60
24	0.79	1.15	0.062	0.05
72	0.39	0.57	0.031	0.03
96	0.35	0.51	0.028	0.02
168	0.27	0.39	0.021	0.02

Appendix D3: Detector linearity

Table 14. Measured and used activities, and corresponding number of 113 keV photons measured in linearity measurements with detector 279.

$A \cdot 10^2$ [MBq]	$\Delta A \cdot 10^2$ [MBq]	$N \cdot 10^5$ [Counts]	$\Delta N \cdot 10^5$ [Counts]
0.18	0.00	0.15	0.007
0.39	0.00	0.13	0.004
0.8	0.00	0.28	0.002
1.6	0.00	0.30	0.003
2.4	0.00	0.46	0.013
3.2	0.00	0.30	0.002
4.0	0.00	0.38	0.002
6.1	0.01	0.33	0.002
16	0.01	0.39	0.004
22	0.01	0.56	0.002
25	0.01	0.61	0.010
40	0.01	0.92	0.014

Table 15. Table with the calculated number of disintegrations and the response for 113 keV photons, determined using values from table 13 (detector 279).

$n \cdot 10^{9}$ [disintegrations]	$\Delta n \cdot 10^{9}$ [disintegrations]	$R \cdot 10^{-2}$ [counts/disintegration]	$\Delta R \cdot 10^{-2}$ [counts/disintegration]
2.3	0.004	6.5	0.3
2.0	0.001	6.5	0.2
4.0	0.002	7.0	0.1
4.0	0.001	7.3	0.1
6.1	0.001	7.6	0.2
4.1	0.001	7.4	0.1
5.1	0.003	7.6	0.0
4.7	0.000	7.0	0.04
6.0	0.000	6.6	0.1
8.3	0.000	6.8	0.02
9.1	0.000	6.7	0.1
15	0.001	6.3	0.1

Table 16. Measured and used activities, and corresponding number of 208 keV photons measured in linearity measurements with detector 279.

$A \cdot 10^{2}$ [MBq]	$\Delta A \cdot 10^{2}$ [MBq]	$N \cdot 10^{5}$ [Counts]	$\Delta N \cdot 10^{5}$ [Counts]
0	0	0.25	0.007
0	0	0.22	0.003
1	0	0.46	0.002
2	0	0.48	0.004
2	0	0.72	0.003
3	0	0.49	0.002
4	0	0.62	0.002
6	0	0.55	0.001
16	0	0.64	0.001
22	0	0.90	0.002
25	0	0.99	0.003
40	0	1.65	0.005

Table 17. Table with the calculated number of disintegrations and the response for 113 keV photons, determined using values from table 15 (detector 279).

$n \cdot 10^{9}$ [disintegrations]	$\Delta n \cdot 10^{9}$ [disintegrations]	$R \cdot 10^{-2}$ [counts/disintegration]	$\Delta R \cdot 10^{-2}$ [counts/disintegration]
4.0	0.006	6.32	0.17
3.5	0.002	6.28	0.09
6.9	0.004	6.63	0.03
6.9	0.002	6.96	0.07
10	0.003	6.96	0.03
7.0	0.001	6.98	0.03
8.7	0.005	7.12	0.02
8.0	0.001	6.80	0.01
10	0.001	6.26	0.01
14	0.001	6.31	0.01
16	0.001	6.34	0.02
25	0.002	6.58	0.02

Table 18. Measured and used activities, and corresponding number of 113 keV photons measured in linearity measurements with detector 276.

$A \cdot 10^2$ [MBq]	$\Delta A \cdot 10^2$ [MBq]	$N \cdot 10^5$ [Counts]	$\Delta N \cdot 10^5$ [Counts]
0.18	0.00	0.16	0.006
0.39	0.00	0.13	0.001
0.79	0.00	0.27	0.001
1.6	0.00	0.29	0.007
2.4	0.00	0.44	0.003
3.2	0.00	0.29	0.006
4.0	0.00	0.37	0.001
6.1	0.01	0.32	0.003
16	0.01	0.39	0.008
22	0.01	0.54	0.002
25	0.01	0.58	0.006
40	0.01	0.92	0.009

Table 19. Table with the calculated number of disintegrations and the response for 113 keV photons, determined using values from table 17.

$n \cdot 10^9$ [disintegrations]	$\Delta n \cdot 10^9$ [disintegrations]	$R \cdot 10^{-2}$ [counts/disintegration]	$\Delta R \cdot 10^{-2}$ [counts/disintegration]
2.3	0.004	6.6	0.27
2.0	0.001	6.4	0.06
4.0	0.002	6.6	0.04
4.0	0.001	7.1	0.16
6.1	0.001	7.2	0.06
4.0	0.001	7.2	0.16
5.1	0.003	7.3	0.03
4.7	0.000	6.8	0.06
6.0	0.000	6.6	0.13
8.3	0.048	6.6	0.06
9.1	0.001	6.4	0.06
15	0.001	6.3	0.06

Table 20. Measured and used activities, and corresponding number of 208 keV photons measured in linearity measurements with detector 276.

$A \cdot 10^2$ [MBq]	$\Delta A \cdot 10^2$ [MBq]	$N \cdot 10^5$ [Counts]	$\Delta N \cdot 10^5$ [Counts]
0	0	0.25	0.006
0	0	0.21	0.001
1	0	0.45	0.002
2	0	0.48	0.003
2	0	0.73	0.000
3	0	0.48	0.002
4	0	0.61	0.001
6	0	0.53	0.002
16	0	0.64	0.000
22	0	0.89	0.003
25	0	0.96	0.003
40	0	1.62	0.002

Table 21. Table with the calculated number of disintegrations and the response for 208 keV photons, determined using values from table 19.

$n \cdot 10^9$ [disintegrations]	$\Delta n \cdot 10^9$ [disintegrations]	$R \cdot 10^{-2}$ [counts/desintergration]	$\Delta R \cdot 10^{-2}$ [counts/disintegration]
4.0	0.006	6.15	0.16
3.5	0.002	6.18	0.03
6.9	0.004	6.55	0.04
6.9	0.002	6.90	0.04
10	0.003	7.01	0.00
7.0	0.001	6.90	0.03
8.7	0.005	7.05	0.01
8.0	0.001	6.56	0.03
10	0.001	6.24	0.01
14	0.082	6.24	0.06
16	0.001	6.17	0.02
25	0.001	6.46	0.01

Appendix D4: Detector efficiency

Detector 279

Table 22. Table with measured and calculated values for determination of the detector efficiency for 113 keV photons.

d [cm]	Δd [cm]	A [MBq]	ΔA [MBq]	$R \cdot 10^3$ [CPS]	$\Delta R \cdot 10^3$ [CPS]	ε [%]	$\Delta\varepsilon$ [%]
7.0	0.1	12.7	0.1	4.41	0.01	67	3
8.0	0.1	12.7	0.1	3.42	0.02	68	3
9.0	0.1	12.7	0.1	2.70	0.01	68	2
10	0.1	12.7	0.1	2.19	0.01	68	2
13	0.1	12.7	0.1	1.41	0.01	68	2
15	0.1	22.6	0.3	2.00	0.00	78	3
20	0.1	22.7	0.3	1.13	0.01	78	3
25	0.1	22.7	0.3	0.71	0.01	77	3
30	0.1	22.7	0.3	0.49	0.00	77	2
35	0.1	22.7	0.3	0.36	0.01	77	3

Table 23. Table with measured and calculated values for determination of the detector efficiency for 208 keV photons

d [cm]	Δd [cm]	A [MBq]	ΔA [MBq]	$R \cdot 10^3$ [CPS]	$\Delta R \cdot 10^3$ [CPS]	ε [%]	$\Delta\varepsilon$ [%]
7.0	0.1	12.7	0.1	5.6	0.00	49	2
8.0	0.1	12.7	0.1	4.4	0.01	51	2
9.0	0.1	12.7	0.1	3.5	0.00	51	2
10	0.1	12.7	0.1	2.8	0.00	51	2
13	0.1	12.7	0.1	1.9	0.01	53	2
15	0.1	22.6	0.3	2.6	0.01	60	2
20	0.1	22.7	0.3	1.5	0.00	61	2
25	0.1	22.7	0.3	1.0	0.00	60	2
30	0.1	22.7	0.3	0.7	0.00	61	2
35	0.1	22.7	0.3	0.5	0.00	60	1

Detector 276

Table 24. Table with measured and calculated values for determination of the detector efficiency for 113 keV photons

d [cm]	*Δd* [cm]	*A* [MBq]	*ΔA* [MBq]	$R \cdot 10^3$ [CPS]	$\Delta R \cdot 10^3$ [CPS]	*ε* [%]	*Δε* [%]
7.0	0.1	12.6	0.1	4.6	0.01	70	3
8.0	0.1	12.6	0.1	3.5	0.01	71	3
9.0	0.1	12.6	0.1	2.8	0.01	72	3
10	0.1	12.6	0.1	2.3	0.01	72	3
13	0.1	12.6	0.1	1.5	0.01	72	2
15	0.1	22.4	0.3	2.1	0.01	83	3
20	0.1	22.4	0.3	1.1	0.01	80	3
25	0.1	22.4	0.3	0.7	0.01	79	3
30	0.1	22.4	0.3	0.5	0.00	79	3
35	0.1	22.4	0.3	0.4	0.00	78	3

Table 25. Table with measured and calculated values for determination of the detector efficiency for 208 kev photons

d [cm]	*Δd* [cm]	*A* [MBq]	*ΔA* [MBq]	$R \cdot 10^3$ [CPS]	$\Delta R \cdot 10^3$ [CPS]	*ε* [%]	*Δε* [%]
7.0	0.1	12.6	0.1	5.3	0.01	47	2
8.0	0.1	12.6	0.1	4.2	0.01	49	2
9.0	0.1	12.6	0.1	3.4	0.01	50	2
10	0.1	12.6	0.1	2.8	0.01	50	2
13	0.1	12.6	0.1	1.8	0.01	52	2
15	0.1	22.4	0.3	2.6	0.01	59	2
20	0.1	22.4	0.3	1.4	0.01	59	2
25	0.1	22.4	0.3	0.9	0.00	58	2
30	0.1	22.4	0.3	0.6	0.00	59	2
35	0.1	22.4	0.3	0.5	0.00	59	2

Appendix E1: Calculations on the field of view

Calculating the angle:

$$\theta = \tan^{-1}\left(\frac{\frac{1}{2}l}{d}\right) \tag{44}$$

Calculating uncertainties

Calculating the uncertainty in the angle:

$$\Delta\theta = \left|\frac{d\theta}{dl}\right| \cdot \Delta l + \left|\frac{d\theta}{dld}\right| \cdot \Delta d \tag{45}$$

$$\Delta\theta = \left|\frac{\frac{1}{2}}{1+\left(\frac{\frac{1}{2}l}{d}\right)^2}\right| \cdot \Delta l + \left|\frac{1}{1+\left(\frac{\frac{1}{2}l}{d}\right)^2} \cdot -\frac{1}{d^2}\right| \cdot \Delta d \tag{46}$$

Appendix E2: Tables with wrist simulation results (t = 0 h)

Table 26. Table with results of the wrist measurement for different distances between detector and wrist (l = 7.2 cm).

E [keV] *d* [cm]	113 $\varphi \cdot 10^2$ [$cm^{-2} \cdot s^{-1}$]	208 $\varphi \cdot 10^2$ [$cm^{-2} \cdot s^{-1}$]	113 $N \cdot 10^4$ [counts]	208 $N \cdot 10^4$ [counts]
0	3.1	4.5	7.1	7.5
2	1.1	1.6	2.5	2.7
4	0.6	0.8	1.2	1.4
6	0.3	0.5	0.7	0.8
8	0.2	0.3	0.5	0.5
10	0.2	0.2	0.3	0.4

Table 27. Table with results of the wrist measurement for different distances between detector and wrist (l = 10 cm).

E [keV] *d* [cm]	113 $\varphi \cdot 10^2$ [$cm^{-2} \cdot s^{-1}$]	208 $\varphi \cdot 10^2$ [$cm^{-2} \cdot s^{-1}$]	113 $N \cdot 10^4$ [counts]	208 $N \cdot 10^4$ [counts]
0	3.6	5.0	8.1	8.4
4	0.7	1.0	1.6	1.7
6	0.4	0.6	1.0	1.1
8	0.3	0.4	0.7	0.7
10	0.2	0.3	0.5	0.5

Table 28. Table with results of the wrist measurement for different distances between detector and wrist (l = 12.5 cm).

E [keV] *d* [cm]	113 $\varphi \cdot 10^2$ [$cm^{-2} \cdot s^{-1}$]	208 $\varphi \cdot 10^2$ [$cm^{-2} \cdot s^{-1}$]	113 $N \cdot 10^4$ [counts]	208 $N \cdot 10^4$ [counts]
0	3.9	5.4	8.7	9.0
2	1.6	2.2	3.5	3.7
4	0.8	1.2	1.9	2.0
6	0.5	0.8	1.2	1.3
8	0.3	0.5	0.8	0.9
10	0.3	0.4	0.6	0.6

Appendix E3: Tables on the wrist simulation results (t = 24 h)

Table 29. Table with results of the wrist measurement for different distances between detector and wrist (l = 7.2 cm).

E [keV] *d* [cm]	113 φ [$cm^{-2} \cdot s^{-1}$]	208 φ [$cm^{-2} \cdot s^{-1}$]	113 *N* [counts]	208 *N* [counts]
0	2.9	5.5	6.7	9.2
2	1.1	2.1	2.5	3.5
4	0.57	1.1	1.3	1.8
6	0.34	0.63	0.78	1.1
8	0.23	0.42	0.51	0.70
10	0.16	0.30	0.36	0.49

Table 30. Table with results of the wrist measurement for different distances between detector and wrist (l = 10 cm).l

E [keV] *d* [cm]	113 φ [$cm^{-2} \cdot s^{-1}$]	208 φ [$cm^{-2} \cdot s^{-1}$]	113 *N* [counts]	208 *N* [counts]
0	7.0	9.8	16	16
2	2.7	3.8	6.0	6.4
4	1.4	2.0	3.1	3.4
6	0.8	1.2	1.9	2.1
8	0.6	0.8	1.3	1.4
10	0.4	0.6	0.90	0.98

Table 31. Table with results of the wrist measurement for different distances between detector and wrist (l = 12.5 cm).

E [keV] *d* [cm]	113 φ [$cm^{-2} \cdot s^{-1}$]	208 φ [$cm^{-2} \cdot s^{-1}$]	113 *N* [counts]	208 *N* [counts]
0	7.5	11	17	18
2	3.0	4.3	6.9	7.3
4	1.6	2.4	3.7	3.9
6	1.0	1.5	2.3	2.4
8	0.68	1.0	1.5	1.7
10	0.49	0.71	1.1	1.2

Appendix E4:Theoretical FOV

Table 32. The calculated field of view needed in correspondence with different arm length and distances between arm and detector.

l [cm]	7.2		10		12.5	
d [cm]	ϑ [°]	FOV [°]	ϑ [°]	FOV [°]	ϑ [°]	FOV [°]
2.0	54.2	108	57	113	57	114
4.0	41.0	82	49	97	52	105
6.0	30.8	62	39	78	45	89
8.0	24.2	48	32	64	37	75
10.0	19.8	40	26	53	32	64

Appendix E5: Measured FOV

Detector 276

Table 33. Tables with result of measurement on the FOV for 113 keV photons.

x [cm]	Δx [cm]	ϑ [°]	$\Delta\vartheta$ [°]	$N \cdot 10^3$ [Counts]	$\Delta N \cdot 10^3$ [Counts]
-7.5	0.2	-36.4	5.1	0	0.1
-6.0	0.2	-30.8	5.4	4	0.1
-4.5	0.2	-24.2	5.6	14	0.1
-3.0	0.2	-16.7	5.7	24	0.2
-1.5	0.2	-8.5	5.8	26	0.0
0.0	0.2	0.0	5.8	25	0.2
1.5	0.2	8.5	5.8	25	0.3
3.0	0.2	16.7	5.7	24	0.2
4.5	0.2	24.2	5.6	17	0.1
6.0	0.2	30.8	5.4	6	0.0
7.5	0.2	36.4	5.1	0	0.0

Table 34. Tables with result of measurement on the FOV for 208keV photons.

x [cm]	Δx [cm]	ϑ [°]	$\Delta\vartheta$ [°]	$N \cdot 10^3$ [Counts]	$\Delta N \cdot 10^3$ [Counts]
-7.5	0.2	-36.4	5.1	0	0.0
-6.0	0.2	-30.8	5.4	5	0.1
-4.5	0.2	-24.2	5.6	17	0.1
-3.0	0.2	-16.7	5.7	29	0.2
-1.5	0.2	-8.5	5.8	31	0.1
0.0	0.2	0.0	5.8	31	0.1
1.5	0.2	8.5	5.8	30	0.4
3.0	0.2	16.7	5.7	29	0.1
4.5	0.2	24.2	5.6	21	0.1
6.0	0.2	30.8	5.4	6	0.1
7.5	0.2	36.4	5.1	0	0.0

Detector 279

Table 35. Tables with result of measurement on the FOV for 113 keV photons.

x [cm]	Δx [cm]	ϑ [°]	$\Delta\vartheta$ [°]	$N \cdot 10^3$ [Counts]	$\Delta N \cdot 10^3$ [Counts]
-7.5	0.2	-36.4	5.1	0	0.0
-6.0	0.2	-30.8	5.4	4	0.1
-4.5	0.2	-24.2	5.6	13	0.1
-3.0	0.2	-16.7	5.7	24	0.2
-1.5	0.2	-8.5	5.8	26	0.1
0.0	0.2	0.0	5.8	26	0.0
1.5	0.2	8.5	5.8	25	0.1
3.0	0.2	16.7	5.7	25	0.1
4.5	0.2	24.2	5.6	17	0.1
6.0	0.2	30.8	5.4	7	0.1
7.5	0.2	36.4	5.1	0	0.1

Table 36. Tables with result of measurement on the FOV for 208 keV photons.

x [cm]	Δx [cm]	ϑ [°]	$\Delta\vartheta$ [°]	$N \cdot 10^3$ [Counts]	$\Delta N \cdot 10^3$ [Counts]
-7.5	0.2	-36.4	5.1	0	0.02
-6.0	0.2	-30.8	5.4	5	0.03
-4.5	0.2	-24.2	5.6	18	0.05
-3.0	0.2	-16.7	5.7	32	0.06
-1.5	0.2	-8.5	5.8	34	0.09
0.0	0.2	0.0	5.8	34	0.24
1.5	0.2	8.5	5.8	33	0.04
3.0	0.2	16.7	5.7	31	0.01
4.5	0.2	24.2	5.6	23	0.03
6.0	0.2	30.8	5.4	8	0.06
7.5	0.2	36.4	5.1	0	0.02